# Multinuclear solid state NMR investigation of hexaniobate and hexatantalate compounds

| | |
|---|---|
| Journal: | *Inorganic Chemistry* |
| Manuscript ID | ic-2016-003459.R2 |
| Manuscript Type: | Article |
| Date Submitted by the Author: | n/a |
| Complete List of Authors: | Deblonde, Gauthier; Lawrence Berkeley National Laboratory, Chemical Sciences Division<br>Coelho Diogo, Cristina; Institut des Materiaux de paris Centre,<br>CHAGNES, Alexandre; ENSCP, IRCP<br>Cote, Gérard; PSL Research University, Chimie ParisTech - CNRS<br>Smith, Mark; Lancaster University, Vice Chancellor's Office<br>Hanna, John; University of Warwick, Department of Physics<br>Iuga, Dinu; University of Warwick, Department of Physics<br>Bonhomme, Christian; Universite Pierre et Marie Curie, |
| | |

# Multinuclear solid state NMR investigation of hexaniobate and hexatantalate compounds

*Gauthier J-P. Deblonde ⊥¶*, Cristina Coelho-Diogo †, Alexandre Chagnes ⊥, Gérard Cote ⊥, Mark E. Smith¥, John V. Hanna|, Dinu Iuga|, Christian Bonhomme ‡*

⊥ *PSL Research University, Chimie ParisTech - CNRS, Institut de Recherche de Chimie Paris, 11 rue Pierre et Marie Curie, 75005 Paris, France*

¶ *ERAMET Research, Hydrometallurgy department, 1 avenue Albert Einstein, F-78193 Trappes, France*

† *Institut des Matériaux de Paris Centre (IMPC-UPMC - FR2482), site collège de France, 75005 Paris, France*

¥ *Vice-Chancellor's Office, University House, Lancaster University, Lancaster, LA14YW, UK*

| *Department of Physics, University of Warwick, Coventry, CV4 7AL, UK*

‡ *Sorbonne Universités, UPMC Univ Paris 06, UMR CNRS 7574, Laboratoire de Chimie de la Matière Condensée de Paris, Collège de France, 11 place Marcelin Berthelot, 75005, Paris, France*

## ABSTRACT

This work determines the potential of solid state NMR techniques to probe proton, alkali and niobium environments in Lindqvist salts. $Na_7HNb_6O_{19},15H_2O$ (**1**), $K_8Nb_6O_{19},16H_2O$ (**2**) and $Na_8Ta_6O_{19},24.5H_2O$ (**3**) have been studied by solid state static and Magic Angle Spinning (MAS) NMR at high and ultra-high magnetic field (16.4 T and 19.9 T). $^1$H MAS NMR was found to be a convenient and straightforward tool to discriminate between protonated and non-protonated clusters $A_xH_{8-x}M_6O_{19},nH_2O$ (A: alkali ion ; M: Nb or Ta). $^{93}$Nb MAS NMR studies at different field and MAS rotation frequency have been performed on (**1**). For the first time, the contribution of $NbO_5O_{\mu 2}H$ sites was clearly distinguished from those assigned to $NbO_6$ sites in the hexaniobate cluster. The strong broadening of the resonances obtained under MAS was interpreted by combining Chemical Shift Anisotropy (CSA) with quadrupolar effects, and by using extensive fitting of the lineshapes. In order to obtain the highest accuracy for all NMR parameters (CSA and quadrupolar), $^{93}$Nb WURST QCPMG spectra under static mode were recorded at 16.4 T for sample (**1**). The $^{93}$Nb NMR spectra were interpreted in connection with the XRD data available in the literature (*i.e.* fractional occupancies of the $NbO_5O_{\mu 2}H$ sites). 1D $^{23}$Na MAS and 2D $^{23}$Na 3QMAS NMR studies of (**1**) revealed several distinct sodium sites. The multiplicity of the sites was again compared to structural details previously obtained by single-crystal X-ray diffraction (XRD) studies. The $^{23}$Na MAS NMR study of (**3**) confirmed the presence of a much larger distribution of sodium sites in accordance with the 10 sodium sites predicted by XRD. Finally, the effect of Nb/Ta substitutions in (**1**) was also probed by multinuclear MAS NMR ($^1$H, $^{23}$Na and $^{93}$Nb).


**KEYWORDS:** Niobium ; Tantalum ; Polyoxometalates ; Solid state NMR

## INTRODUCTION

Niobium (Z = 41) and tantalum (Z = 73) are strategic metals for alloys and electronic industries and are classified as critical metals due to the few locations where both metals are extracted and because of their use in several applications including alloys for the automotive, aerospace and nuclear industries, electronic component, superconducting magnets, etc.[1] Whereas classical and economical routes to recover Nb and Ta from natural ores require fluoride media;[2,3] the development of innovative and sustainable processes to recover Nb and Ta could not be achieved in such media owing to the environmental and health risks inherent to fluoride solutions. In this regard, alkaline media have recently received growing attention for Nb and Ta recovery as high solubility of Nb(V) and Ta(V) can be obtained along with separation from impurities such Fe, Mn and Ti.[4–6]

Niobium and tantalum speciation in alkaline media has been studied since the 19$^{th}$ Century[7] and widely debated during the 20$^{th}$ Century but the chemistry of both group V metals is still challenging and rather unexplored compared to other metals such as molybdenum or tungsten and even the lightest group V vanadium. Among a broad variety of polyoxometalates[8] that can be formed with Nb(V) and Ta(V) in basic media, the Lindqvist salts, namely $A_xH_{8-x}Nb_6O_{19},nH_2O$ and $A_xH_{8-x}Ta_6O_{19},nH_2O$ (A = Li, Na, K, Rb, Cs, tetramethylammonium or tetrabutylammonium ; $0 \leq x \leq 4.5$), are of high importance. Indeed, the Lindqvist ions $H_xNb_6O_{19}^{x-8}$ and $H_xTa_6O_{19}^{x-8}$ are the dominant species of Nb and Ta in aqueous solutions at pH $\geq$ 10.[9,10] Moreover, in the solid state, the Lindqvist salt was the first polyoxoniobate to be isolated and characterized thanks to its stability and relatively easy synthesis.[11] The industrial recovery of Nb and Ta by caustic leaching of natural ores was also explained by the formation of

the hexameric ions $M_6O_{19}^{8-}$ (M = Nb, Ta) highlighting the robustness of the $M_6O_{19}$ framework and its importance in future niobium and tantalum industries.[12,13]

The structure of the Lindqvist ion $M_6O_{19}$, has been extensively studied and consists of a super octahedron of 6 edge-sharing and distorted octahedra $MO_6$. The $M_6O_{19}$ cluster has 3 different types of oxygen with one central atom $\mu_6$-O inside an $M_6O$ octahedra, six terminal oxygens $\eta$=O and twelve bridging oxygens $\mu_2$-O (Figure 1).

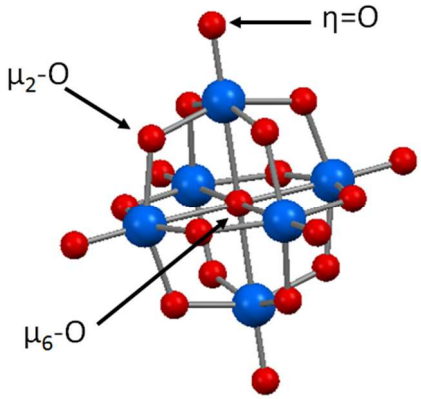


**Figure 1.** Representation of the Lindqvist ion $M_6O_{19}$ (Red spheres: oxygen; Blue spheres: niobium or tantalum) containing 1 central oxygen ($\mu_6$-O), 6 terminal oxygens ($\eta$=O) and 12 bridging oxygens ($\mu_2$-O).

As a consequence of their easy accessibility, most of the studies related to Nb(V) and Ta(V) speciation in alkaline media (in both the solid state and solution) are based on hexaniobate or hexatantalate salts. Although pioneering works were focused on potassium and sodium salts, the chemistry of hexaniobate and hexatantalate salts have recently been extended to their lithium, rubidium, cesium and quaternary ammonium counterparts (Table 1). Due to the several degrees of freedom that the chemical formula $A_xH_{8-x}M_6O_{19},nH_2O$ exhibits, an important series of

hexaniobate and hexatantalate salts are reported even if some of them were not fully characterized.

**Table 1:** List of hexaniobate and hexatantalate salts reported in the literature.

| Compound | Space group | Reference |
|---|---|---|
| $Li_8Ta_6O_{19},24H_2O$ | | [14] |
| $Na_6Li(H_3O)Ta_6O_{19},14H_2O$ | *Pnnm* | [15]* |
| $Na_8Ta_6O_{19},26H_2O$ | *P6₃* and *R-3* | [16]* |
| $Na_8Ta_6O_{19},24.5H_2O$ | *P6₃* | [17]* - [18] |
| $Na_8Ta_6O_{19},24H_2O$ | | [19] |
| $Na_8Ta_6O_{19},15H_2O$ | *Pmnn* | [19] - [20]* |
| $K_7NaTa_6O_{19},14H_2O$ | *P2₁* | [21]* - [22] |
| $K_8Ta_6O_{19},17H_2O$ | | [15] - [23] - [24] - [25] - [26] |
| $K_8Ta_6O_{19},16H_2O$ | *Cc* | [21]* - [27] - [28] - [29] - [30] |
| $K_8Ta_6O_{19},12H_2O$ | | [30] |
| $K_8Ta_6O_{19},9H_2O$ | | [30] |
| $K_8Ta_6O_{19},4H_2O$ | | [30] |
| $Rb_6Na_2Ta_6O_{19},21H_2O$ | *R-3* | [20]* |
| $Rb_8Ta_6O_{19},14H_2O$ | *P2₁/n* | [31] |
| $Rb_8Ta_6O_{19},4H_2O$ | *C2/c* | [31] |
| $Rb_8Ta_6O_{19}$ | | [31] |
| $Cs_8Ta_6O_{19},14H_2O$ | *P2₁/n* | [31] |
| $Cs_8Ta_6O_{19}$ | *I4/m* | [31] |
| $TBA_{3.5}[H_{4.5}(Ta_6O_{19})],2THF,5.5H_2O$ | $P\bar{1}$ | [32] |
| $TBA_6H_2Ta_6O_{19},10H_2O$ | *P2₁/c* | [24] - [33] |
| $Li_8Nb_6O_{19},22H_2O$ | | [14] |
| $Li_8Nb_6O_{19},15.5H_2O$ | *P 21/c* | [34]* |
| $Li_6H_2Nb_6O_{19},14H_2O$ | | [34] |
| $KLi_7Nb_6O_{19},15H_2O$ | *P2₁/n* | [20]* |
| $Na_6LiHNb_6O_{19},15H_2O$ | *Pnnm* | [15]* |
| $Na_7HNb_6O_{19},15H_2O$ | *Pmnn* | [18] - [20]* - [35] - [36] - [37] - [38] - [39] - [40] |
| $Na_7HNb_6O_{19},14H_2O$ | | [41] |
| $Na_8Nb_6O_{19},13H_2O$ | | [42] - [43] |
| $K_4Na_4Nb_6O_{19},9H_2O$ | | [43] |
| $K_7HNb_6O_{19},16H_2O$ | | [23] |
| $K_7HNb_6O_{19},13H_2O$ | | [15] - [25] - [26] - [35] - [38] - [44] - [45] |
| $K_7HNb_6O_{19},10H_2O$ | *C2/c* | [46]* |
| $K_8Nb_6O_{19},16H_2O$ | *C2/c* | [46]* - [47] - [48] |
| $K_8Nb_6O_{19},10H_2O$ | | [43] |

| | | |
|---|---|---|
| $K_6H_2Nb_6O_{19},13H_2O$ | | [49] - [50] |
| $Rb_8Nb_6O_{19},14H_2O$ | *P2₁/n* | [46]* |
| $Rb_6H_2Nb_6O_{19},19H_2O$ | *R-3* | [46]* |
| $Rb_6H_2Nb_6O_{19},9H_2O$ | *P-1* | [46]* |
| $Cs_6Na_2Nb_6O_{19},18H_2O$ | *R-3* | [46]* |
| $Cs_6H_2Nb_6O_{19},9H_2O$ | *P2₁/c* and *Pbca* | [46]* |
| $Cs_8Nb_6O_{19},14H_2O$ | *P2₁/n* | [46]* |
| $TMA_5[H_3Nb_6O_{19}],20H_2O$ | *I 2/a* | [51]* |
| $TMA_8[Nb_6O_{19}],15H_2O$ | | [52] |
| $TBA_4[H_4Nb_6O_{19}],7H_2O$ | | [53] |

*: asterisk indicates the paper were the crystal structure was solved. TMA: tetramethylammoniun. TBA: tetrabutylammonium.

Even though, hexaniobate and hexatantalate salts have been known for a long time, the full resolution of their crystal structure was performed in the last two decades with important contributions from Nyman's and Hartl's groups. For the sodium hexaniobate salt, the structure $Na_7(H_3O)Nb_6O_{19},14H_2O$ was first proposed by Goiffon *et al.* in 1980[40] and corrected recently to $Na_7HNb_6O_{19},15H_2O$ by Nyman's group based on NMR studies (including $^{17}O$ in solution state).[20,36] The very recent advances in the characterization of Nb and Ta Lindqvist salts and other polyoxometalates reflect the complexity of Nb and Ta chemistry and underline the need for developing new techniques to probe such compounds.

In this regard, solid state Magic Angle Spinning Nuclear Magnetic Resonance (MAS NMR) seems to be potentially important for studying hexaniobate and hexatantalate salts. In particular, the alkali hexaniobate salts offer a unique class of compounds with multiple nuclei that can be probed by solid state MAS NMR, namely $^{1}H$, $^{6}Li$, $^{7}Li$, $^{17}O$, $^{23}Na$, $^{87}Rb$, $^{133}Cs$ and $^{93}Nb$. Although several techniques were used to investigate hexaniobate and hexatantalate salts, only a few articles[20,36,46,54] were published on $^{1}H$, $^{6/7}Li$, and $^{93}Nb$ solid state MAS NMR and no $^{23}Na$, $^{87}Rb$, or $^{133}Cs$ NMR studies were performed for such salts to date.

This work underlines the potential of MAS NMR technique to probe proton, alkali and niobium environments in Lindqvist salts. The $^{1}$H MAS NMR studies of $Na_7HNb_6O_{19},15H_2O$ (**1**), $K_8Nb_6O_{19},16H_2O$ (**2**) and $Na_8Ta_6O_{19},24.5H_2O$ (**3**) presented in this article illustrate the ability to distinguish between *protonated* and *non-protonated* clusters with this technique. Under fast MAS (30 kHz), the contribution of the water molecules and $NbO_5O_{\mu 2}H$ groups (if present) to the $^{1}$H MAS or synchronized echo MAS experiments were clearly resolved.

$^{93}$Nb MAS and static NMR was so far mainly applied to the characterization of several families of Nb-containing materials[54–56] but rarely to hexaniobate salts.[54] More specifically, *non-protonated* $[Nb_6O_{19}]^{8-}$ clusters in $K_8Nb_6O_{19}.16H_2O$ were investigated at ultra-high magnetic field. In this particular case, three non-equivalent Nb sites were expected based on the crystallographic structure. Nevertheless, all $^{93}$Nb static and MAS NMR spectra could be reasonably interpreted with a *unique* set of CSA and quadrupolar parameters (see below). In other words, the spectral resolution was not enough to distinguish all individual $^{93}$Nb sites. To the best of our knowledge, no $^{93}$Nb NMR parameters have been published so far for $NbO_5O_{\mu 2}H$ entities and we present here the first complete sets of parameters for such groups. Most importantly, we demonstrate that $NbO_5O_{\mu 2}H$ groups were distinguished on the basis of their characteristic quadrupolar parameters ($C_Q(^{93}Nb)$) and *not* their isotropic chemical shift, $\delta_{iso}(^{93}Nb)$. The full interpretation of the NMR spectra was related to the corresponding XRD data. Very interestingly, highly resolved $^{23}$Na MAS NMR spectra (related to small $C_Q(^{23}Na)$) were sensitive to the small variations in the local order around the sodium atoms. Distributions of $\delta_{iso}(^{23}Na)$ could be related to order/disorder in the crystallographic structures. The doping of hexaniobate sodium salts with tantalum ($Na_7HNb_{6-x}Ta_xO_{19},15H_2O$ with $x \leq 0.33$) did not significantly influence the $^{93}$Nb spectra whereas $^{23}$Na spectra were modified demonstrating again

the particular sensitivity of this technique. The effect of Ta insertion in $Na_7HNb_6O_{19},15H_2O$ (**1**) was finally compared with the crystal structures of the isostructural salts, $Na_7HNb_6O_{19},15H_2O$ (**1**) and $Na_8Ta_6O_{19},15H_2O$.

## EXPERIMENTAL SECTION

**Materials.** Water used in this study was purified through a Millipore DI-pak® and a Millipore Simpak®2 systems (R>18.2 MΩ.cm). Acetonitrile (99.9%), NaOH and KOH were purchased from VWR. $Nb_2O_5$ (99.9%) and $Ta_2O_5$ (99.99%) were purchased from Aldrich. $NbCl_5$ (99%) was purchased from Alfa Aesar.

**Synthesis of $Na_7HNb_6O_{19},15H_2O$ (1).** 30.0 g of NaOH pellets were finely ground and mixed with 10.0 g of $Nb_2O_5$. The mixture was placed in a Pt crucible and heated to 450 °C for 5 h. After cooling to room temperature, the calcinate was successively washed with 2*250 mL and 3*100 mL of water. The solid was then recrystallized as follows. About 20 g of solid were dissolved in 300 mL of water at ~90 °C. After hot filtration, the filtrate was gently cooled down to room temperature so that, after about 2 hours, fine crystals appear on the walls and at the bottom of the chiller. The colorless crystals were recovered by Büchner filtration and washed with 20 mL of water and 20 mL of absolute ethanol. The crystals were then dried in air for 48 h. SEM images of crystals (**1**) are given in the supporting information (Figure S1). In order to check the elimination of NaOH excess, required by the alkaline fusion, the ratio Nb/Na were measured by ICP-AES in the different steps of the synthesis. This yielded a Na/Nb molar ratio of > 10,000 (washing 1), 23.9 (washing 2), 2.83 (washing 3), 1.80 (washing 4), 1.82 (washing 5) 1.17 (recrystallization filtrates) and 1.17 (salt). The product was identified as $Na_7HNb_6O_{19},15H_2O$ by powder X-ray diffraction, Raman and infrared spectroscopies. The yield

was 38 % based on Nb. Elemental analysis for $Na_7HNb_6O_{19},15H_2O$, calculated (wt%): 20.9 $H_2O$, 12.4 Na, 43.1 Nb. Found: 21.5 $H_2O$, 12.0 Na, 41.6 Nb. Raman ($cm^{-1}$): 904 ; 837 ; 769 ; 524 ; 485 ; 458 ; 380 ; 278 ; 215 ; 172. IR ($cm^{-1}$): 3226 (vs) ; 1658 (m) ; 1631 (m) ; 847 (s) ; 756 (s) ; 692 (vs) ; 617 (s). Raman spectrum and TGA analyses are given in Figures S2 and S3.

**Synthesis of $K_8Nb_6O_{19},16H_2O$ (2).** In this contribution, sample **(2)** will be of particular help for the interpretation of $^1H$ MAS NMR spectra (see below). This compound was synthesized starting from $NbCl_5$, as detailed elsewhere.[9] $K_8Nb_6O_{19},16H_2O$ was identified by power X-ray diffraction, Raman and infrared spectroscopies. Elemental analysis for $K_8Nb_6O_{19},16H_2O$, calculated (wt%): 19.7 $H_2O$, 21.4 K, 38.1 Nb. Found: 19.6 $H_2O$, 20.7 K, 36.2 Nb. Raman ($cm^{-1}$): 875 ; 827 ; 745 ; 530 ; 459 ; 376 ; 288 ; 217. IR ($cm^{-1}$): 3222 (vs) ; 1653 (m) ; 1631 (m) ; 847 (s) ; 697 (vs) ; 617 (m). Raman spectrum and TGA analysis are given in Figures S4 and S5.

**Synthesis of $Na_8Ta_6O_{19},24.5H_2O$ (3).** The synthesis was inspired from Abramov *et al*.[17] 5.9 g of NaOH pellets were finely ground and mixed with 3.3 g of $Ta_2O_5$. The mixture was placed in a Pt crucible and heated to 450 °C for 5 h. The purification of the calcinate was performed similarly to $Na_7HNb_6O_{19},15H_2O$ synthesis. SEM images of (**2**) crystals are given in supporting information (Figure S6). The yield was 44 % based on Ta. Elemental analysis for $Na_8Ta_6O_{19},24.5H_2O$, calculated (wt%): 21.9 $H_2O$, 9.1 Na, 53.9 Ta. Found: 22.0 $H_2O$, 8.9 Na, 51.9 Ta. Raman ($cm^{-1}$): 861 ; 754 ; 511 ; 420 ; 346 ; 213 ; 187 ; 172. IR ($cm^{-1}$): 3226 (vs) ; 1657 (m) ; 831 (s) ; 767 (s) ; 692 (vs) ; 617 (s). Raman spectrum and TGA analysis are given in Figures S7 and S8.

**Solid state MAS NMR at high and ultra-high magnetic field.** Solid State NMR experiments were performed on: *(i)* a Bruker AVANCE III 700 spectrometer at 16.4 T ($\nu_0(^1H)$ = 700 MHz,

$\nu_0(^{23}Na)$ = 185.22 MHz, $\nu_0(^{93}Nb)$ = 171.39 MHz) with 2.5 mm (30 kHz), 1.3 mm (65 kHz) double resonance Bruker MAS probes and 5mm Bruker static probe.. Samples were spun at the magic angle using $ZrO_2$ rotors**.** *(ii)* a Bruker AVANCE II 850 spectrometer at 19.9 T ($\nu_0(^1H)$ = 850 MHz, $\nu_0(^{23}Na)$ = 224.91 MHz, $\nu_0(^{93}Nb)$ = 208.12 MHz) with a 1 mm (80 kHz) double resonance Jeol MAS probe. $^1H$ MAS spectra were obtained by using Single Pulse Experiment (SPE) ($t_{90°}(^1H)$ = 3.0 µs for the 2.5 mm MAS probe) and synchronized Hahn echo for spectral editing (two pulses sequence: $p_1$-τ-$p_2$ with $p_1$ = 3.0 µs and $p_2$ = 6.0 µs, with a 16 **step** phase cycling). The longest interpulse delay corresponded to 10 rotor periods. For quantitative purposes, all 1D $^{23}Na$ (I = 3/2) MAS NMR spectra were obtained by using short pulses (< π/8). Nutation curves were first established by using a solution of 1M $NaCl_{(aq)}$ ($t_{90°}(^{23}Na)$ = 8.8 µs for the 2.5 mm MAS probe). $^{93}Nb$ WURST QCPMG[57] spectra were obtained by using a 5mm static probe. As the sensitivity of the experiment was high, no DFS enhancement technique[58] was implemented. The WURST shape was defined as follows: sweep width of 1000 kHz (during 45 µs), definition by 1000 points. The power of the RF field was then the only optimized parameter (here, ~ 10 W). Probe contributions to the final signals were carefully checked under the same experimental conditions. Finally, potential effects of the irradiation offset for $^{93}Nb$ were explored as well (see the Discussion section below). 2D $^{23}Na$ 3QMAS NMR spectra[59] were obtained by using the amplitude modulated Z-filter experiment ($p_1$-$t_1$(3Q evolution)-$p_2$-τ-$p_3$-$t_2$(acquire)).[60] The optimized pulse lengths of the 3Q excitation ($p_1$) and reconversion ($p_2$) were $p_1$ = 4.0 µs, $p_2$ = 2.0 µs, respectively, implemented with an RF field of 85 kHz, whereas the soft π/2 Z-filter ($p_3$) was set to 40 µs, which was delivered with an RF field of ~ 3 kHz. Synchronized echoes (the interpulse delay was always set to one rotor period) with short pulses (π/10) were used as well for $^{93}Nb$ (I = 9/2) MAS NMR ($t_{90°}(^{93}Nb)$ = 4.0 µs for a saturated solution of $NbCl_5$

in acetonitrile using the 1.3 mm MAS probe and $t_{90°}(^{93}Nb)$ = 12.0 μs for the 2.5 mm MAS probe). As protons are present in all structures, systematic investigation of the effects of $\{^1H\}$ decoupling on $^{23}Na$ and $^{93}Nb$ spectra was performed. Tiny effects on spectral resolution were observed so that mainly undecoupled $^1H$ spectra were recorded in this study. In terms of $^1H$ homonuclear decoupling, and in order to further increase the $^1H$ spectral resolution, optimized DUMBO (Decoupling Using Mind-Boggling Optimization) sequence was implemented at lower MAS frequency (12 kHz).[61] No increase in resolution was observed for compounds **(1)**, **(2)** and **(3)**.

$^1H$ and $^{23}Na$ NMR chemical shift were referenced to TMS (tetramethylsilane) (*via* solid adamantane), and a solution of 0.1M $NaCl_{(aq)}$, respectively. As a convenient secondary chemical shift reference, a powder sample of NaCl was also used (+7.25 ppm). $^{93}Nb$ NMR chemical shifts were referenced to a saturated solution of $NbCl_5$ in acetonitrile at 0.0 ppm. Lapina *et al.*[54] used this reference, whereas Hanna *et al.*[55] used the following solution as a chemical shift reference: $K[NbCl_6]/CH_3CN$. A solution of $NbCl_5$ in acetonitrile without KCl exhibits three peaks. The most deshielded peak is sharp, the second peak is broader and shifted by about -55 ppm and the third peak is sharp and shifted by about -494 ppm. The second peak disappears after several hours. These three peaks were attributed to the equilibrium between $NbCl_5$, $NbCl_6^-$ and $NbCl_4^+$. The value of 0 ppm was attributed to the most deshielded peak (*i.e.* $NbCl_6^-$**).** All MAS experiments were performed without any temperature control of the samples. The expected increase in temperature was the following: $T_{sample} \approx 45$ °C for a 2.5 mm probe at 30 kHz and 40 °C for a 1.3 mm probe at 65 kHz.

All decompositions of spectra were performed using the DMfit software available free of charge online.[54] For $^1H$ spectra, Lorentz/Gaussian (*L/G*) lineshapes were used. For $^{23}Na$ spectra,

the *Qmas1/2* option was used corresponding to the central transition (broadened by eventual second-order quadrupolar effects) under the assumption of *infinite* MAS rotation frequency (no spinning sidebands). For $^{93}$Nb, previous studies have clearly demonstrated the combined role of quadrupolar interaction and CSA on the lineshapes, especially at high magnetic field.[54,55] Consequently, the *int2QUAD* DMfit module was used under the assumption of *finite* rotation frequency for the central transitions. In order to accurately quantify the spectra, the contribution of the satellites was taken into account in the region of the central transition resonances (the corresponding lineshapes were obtained far from the isotropic regions of interest where the contributions of the spinning sidebands of the central transitions are negligible). The following parameters were taken into account for each $^{93}$Nb site: $\delta_{iso}(^{93}Nb)$, CSA (including the anisotropy, $\delta_{CSA}$, and the asymmetry, $\eta_{CSA}$), $C_Q(^{93}Nb)$, $\eta_Q(^{93}Nb)$ and the set of Euler angles between both tensors. The following conventions holded.[62] The Electric Field Gradient (EFG) was characterized by $V_{xx}$, $V_{yy}$, $V_{zz}$ with $|V_{yy}| \leq |V_{xx}| \leq |V_{zz}|$ and $V_{xx} + V_{yy} + V_{zz} = 0$, $C_Q = eQV_{zz}/h$, $\eta_Q = (V_{yy} - V_{xx})/V_{zz}$ with $0 \leq \eta_Q \leq 1$. CSA was characterized by $\delta_{11}$, $\delta_{22}$, $\delta_{33}$ with $|\delta_{33} - \delta_{iso}| > |\delta_{11} - \delta_{iso}| > |\delta_{22} - \delta_{iso}|$, $\delta_{iso} = 1/3\ (\delta_{11} + \delta_{22} + \delta_{33})$, $\delta_{CSA} = \delta_{33} - \delta_{iso}$ (anisotropy), $\eta_{CSA} = |(\delta_{22} - \delta_{11}) / \delta_{CSA}|$ (asymmetry). The set of Euler angles $\{\varphi,\chi,\Psi\}$ oriented the CSA tensor in the quadrupolar tensor principal axes system. Full experimental details (*e.g.*, rotor diameter: Ø, MAS frequency: $\nu_{rot}$, number of scans: NS, recycle delay: RD, line broadening: LB) are systematically shown in the Figure captions.

## RESULTS AND DISCUSSION

### $^1$H MAS NMR.

Three different Lindqvist salts $Na_7HNb_6O_{19},15H_2O$ (**1**), $K_8Nb_6O_{19},16H_2O$ (**2**) and $Na_8Ta_6O_{19},24.5H_2O$ (**3**) were investigated by 1D $^1H$ MAS NMR. The sodium hexaniobate salt (**1**) has fifteen water molecules surrounding the $Nb_6O_{19}$ cluster and only one proton bound to the cluster by one bridging oxygen $\mu_2$-O ($NbO_5O_{\mu 2}H$ site) (Figure 1). The structure of (**1**) was extensively studied by Alam *et al*.[36] using $^1H$ MAS, $^1H$-$^{93}Nb$ TRAPDOR (TRAnsfer of Population in Double Resonance)[63] and solution state $^{17}O$ NMR experiments. The $^1H$ MAS NMR spectrum of (**1**) has a sharp peak at + 1.9 ppm and a much broader broad peak centered at + 6.3 ppm (Figure 2) in agreement with Alam *et al*. The large peak at + 6.3 ppm was assigned to the water molecules and the sharp peak at + 1.9 ppm to the proton bound to $NbO_5O_{\mu 2}H$ sites. The Nb-OH resonance is strongly shielded as a consequence of the geometry of the local H-bond networks.[64] Indeed, the variation of $\delta_{iso}(^1H)$ could be easily related to the minimum OH···O distance with the following rule: $\delta_{iso}(^1H)$ decreased strongly upon increasing the OH···O distance. In other words, protons in Nb-OH groups are rather isolated leading to the net shielding of $\delta_{iso}(^1H)$ when compared to protons in water molecules.

Using a Hahn echo MAS NMR experiment (Figure 2), it was possible to clearly distinguish the $NbO_5O_{\mu 2}H$ resonance by $T_2(^1H)$ filtering. It allowed to extract precise line shapes and $\delta_{iso}(^1H)$ values for the whole $^1H$ spectrum. It has to be noticed that the broad OH resonance is actually much more complex than a simple Lorentzian lineshape. It corresponds probably to the sum of individual components with variable $T_2(^1H)$. It follows that accurate quantification of the two components ($\delta_{iso}(^1H)$ = + 6.3 and + 1.9 ppm) was difficult to obtain. Nevertheless, this simple approach is sufficient to distinguish between $NbO_5O_{\mu 2}H$ groups and water molecules resonances. We finally mention that this analysis is in agreement with results already published by Alam *et al*.[36]. The authors used $T_2(^1H)$ based editing techniques as well as double quantum filtering to

achieve realistic assignments. We further observe that spinning faster at the magic angle (> 30 kHz) didn't lead to significant increase in resolution demonstrating that for 30 kHz ≤ $\nu_{rot}$, $^1$H-$^1$H homonuclear dipolar coupling were efficiently averaged leaving only isotropic $^1$H chemical shifts distributions (mainly related to protons in water molecules).

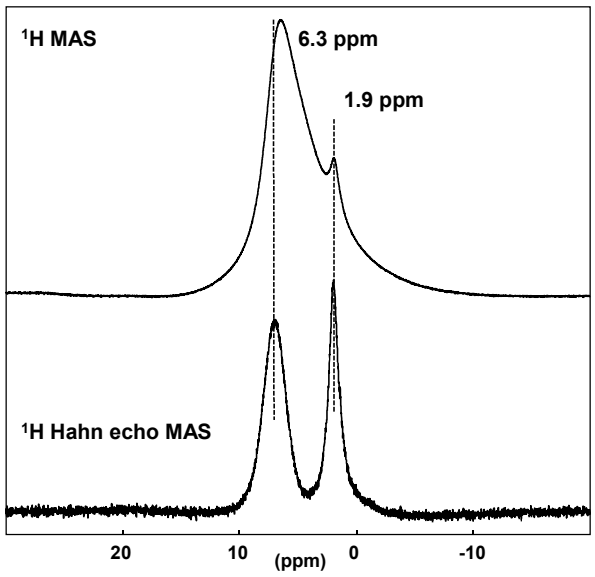


**Figure 2:** $^1$H MAS and Hahn echo MAS NMR spectra of $Na_7HNb_6O_{19},15H_2O$ (**1**). See Table S1 for NMR parameters. Vertical dashed lines are guides for the eye only (showing the complexity of the broad line centered at + 6.3 ppm).

In order to further compare protonated and non-protonated clusters, solid state $^1$H NMR spectra of (**2**) and (**3**) were recorded (Figure 3). The $^1$H NMR peaks related to the water molecules present in (**2**) and (**3**) are much sharper when compared to the broad peak found for $Na_7HNb_6O_{19},15H_2O$ (**1**). Moreover, no shielded resonance (< 2 ppm) was observed for these derivatives. Contrary to the alkali hexaniobate salts, no protonated hexatantalate alkali salts have been reported so far (see Table 1). This is mainly due to the lower pKa of the couple $HTa_6O_{19}^{7-}$ /$Ta_6O_{19}^{8-}$ compared to $HNb_6O_{19}^{7-}$/$Nb_6O_{19}^{8-}$.[10,22] Consequently, the rather sharp $^1$H peak observed for (**3**) cannot arise from protons linked to the hexatantalate cluster. The similarity between the

$^{1}$H NMR spectra of $K_8Nb_6O_{19},16H_2O$ (**2**) and of $Na_8Ta_6O_{19},24.5H_2O$ **(3)** also suggested that a sharp $H_2O$ peak at ~ + 4.5 ppm was only obtained for non-protonated salts. It is also interesting to note that Nyman *et al.*[46] mentioned that $^{1}$H MAS NMR spectra of the protonated salts $Rb_6H_2Nb_6O_{19,}9H_2O$ and $Cs_6H_2Nb_6O_{19,}9H_2O$ exhibited also a broad resonance around + 5 ppm related to water molecules. The broad resonance at around + 5 ppm was also observed by Alam et al.[65] for the protonated slats $Rb_6(H_3O)_2Nb_6O_{19},17H_2O$ and $K_7HNb_6O_{19},10H_2O$. To our knowledge, no $^{1}$H NMR spectra of the water molecules of fully deprotonated hexaniobate or hexatantalate clusters have been reported in the literature. The observation of a rather sharp $H_2O$ peak for (**2**) and (**3**) could suggest that the water molecules are subjected to local motion in their crystal lattice. As a consequence, the $^{1}$H-$^{1}$H homonuclear dipolar interactions are partially averaged at room temperature leading to much sharper $^{1}$H resonances. NMR spectra presented in Figure 3 suggests that all the $H_2O$ molecules in (**2**) and (**3**) are not equivalent. Based on the available XRD data, six water molecules are expected in the asymmetric unit of **(2)**. In the case of **(3)**, the positions of the water molecules are not located in the published XRD structure but several non-equivalent water molecules are expected given the complex structure of this compound (see $^{23}$Na NMR section below). Attempts to improve the resolution of the $^{1}$H signal by DUMBO acquisition (see the Experimental section) did not lead to significant improvement in the spectral resolution (the DUMBO sequence promotes efficient averaging of the strong $^{1}$H-$^{1}$H homonuclear couplings). It is assumed here that local motion of the protons lowered drastically the efficiency of the DUMBO sequence. Moreover, an interesting correlation could be established between the $^{1}$H MAS NMR spectra and the TGA of samples **(1)**, **(2)** and **(3)** (see SI for TGA curves). In the case of **(1)**, water protons (and $NbO_5O_{\mu 2}H$) participate to a rather rigid H-bond network, as shown by the broad $^{1}$H resonance at + 6.3 ppm. On the TGA curve, the loss

of almost all water molecules was observed at T ~ 125 °C. It is expected from Figure 3, that partial averaging of the $^{1}$H-$^{1}$H homonuclear dipolar interaction should lead to a less rigid H-bond network. Indeed, the loss of water molecules occurred at lower T (~ 90 °C) for **(2)** and **(3)**. Rather unexpectedly, the global $^{1}$H linewidths for (**2**) and (**3**) were comparable, indicating similar proton local dynamics in both samples. However, we stress on the fact that the *average* proton chemical shifts for (**2**) and (**3**) were clearly separated (difference of ~ 0.75 ppm). This demonstrated the extreme sensitivity of this particular NMR parameter towards the chemical nature of the metal in the oxo-clusters and the alkaline counter-cation. It follows that $\delta_{iso}(^{1}H)$, though averaged through dynamical processes, should be a pertinent indicator for detailed analysis of metal derived oxo-clusters.

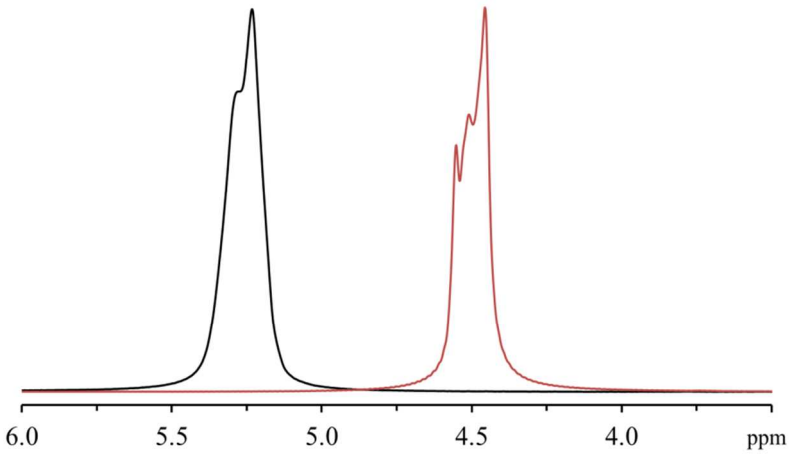


**Figure 3.** $^{1}$H MAS NMR spectra of $K_8Nb_6O_{19},16H_2O$ (**2**) (black) and of $Na_8Ta_6O_{19},24.5H_2O$ (**3**) (red). See Table S1 for NMR parameters.

The use of $^{1}$H MAS and Hahn echo MAS NMR for identification of protonated or deprotonated hexaniobate and hexatantalate salts is straightforward compared to other techniques such as Raman spectroscopy.[66] Due to the variety of the hexametalate salts that have been reported in the

literature (see Table 1) and the difficulty in identifying the protonation state of such salts, fast MAS NMR represents a powerful tool which can supplement the bond-valence sum (BVS) calculations, or bond length examinations traditionally used to ruled out the presence of protons bound to the cluster**.**

**$^{93}$Nb echo MAS NMR.**

$^{93}$Nb is another nucleus found in hexaniobate salts that can be probed by solid state NMR. Thanks to its natural abundance (100 %) and its relatively high content in hexaniobate salts (~25 to ~50 wt %), $^{93}$Nb MAS NMR spectra with good signal-to-noise ratio can be obtained in only a few hours. Nonetheless, $^{93}$Nb has a high nuclear spin (I = 9/2) and a large quadrupole moment (-0.32 barn) which complicate the use of NMR techniques to study this particular nuclei. Most of the works published on $^{93}$Nb MAS NMR were performed on niobium oxides[55] or mixed-metal oxides that are used as catalysts, piezoelectric components or optoelectronic materials.[54,67–71]

To the best of our knowledge, the only $^{93}$Nb static/MAS NMR study performed on a hexaniobate salt has been published recently by Lapina *et al*.[54] Based on the reported crystallographic structure,[46] altogether with the static and MAS NMR spectra recorded at high magnetic field (21.1 T), the $^{93}$Nb NMR parameters of $K_8Nb_6O_{19},16H_2O$ (**2**) were determined. The authors reported that the three non-equivalent niobium sites present in (**2**) were practically indistinguishable and that their NMR frequencies could almost be described by a *unique* $^{93}$Nb site with: $\delta_{iso}(^{93}Nb)$ = - 920 ppm, $C_Q$ = 42 MHz and $\eta_Q$ = 0.0. The authors also revealed that the calculated NMR parameters ($\delta_{iso}(^{93}Nb)$) for the cluster $Nb_6O_{19}^{8-}$ surrounded by height $K^+$ did not significantly differ from the NMR parameters calculated for $Nb_{10}O_{28}^{6-}$ surrounded by six

protons. In other words (and based mainly on *ab initio* calculations), it seemed difficult to distinguish $NbO_5O_{\mu 2}H$ from $NbO_6$ groups relying only on isotropic chemical shift. We studied here $Na_7HNb_6O_{19},15H_2O$ (**1**) by $^{93}Nb$ echo MAS NMR. Even when using very fast MAS at ultra-high magnetic fields, the approximation of infinite MAS rotation frequency did not apply here. Indeed, spinning sidebands of central transitions were clearly observed (see Figure 4).

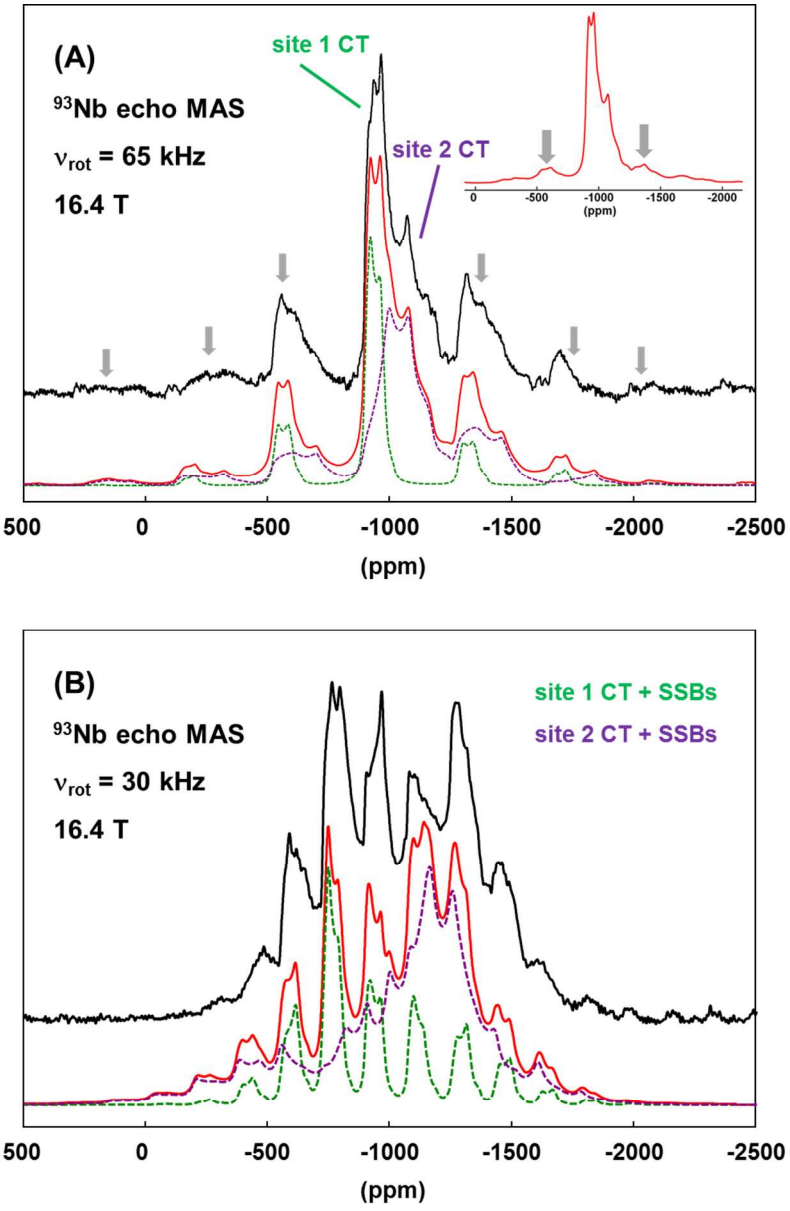

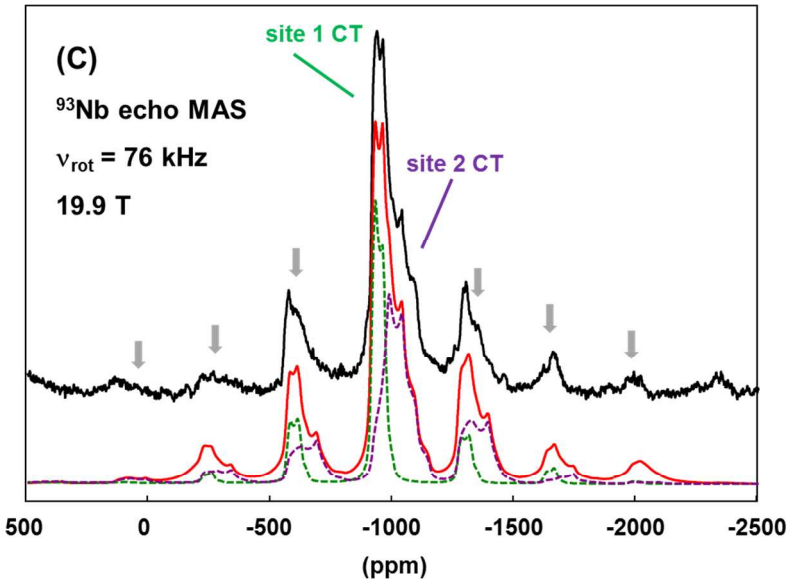


**Figure 4:** $^{93}$Nb echo MAS NMR spectra of $Na_7HNb_6O_{19},15H_2O$ (**1**). **(A)**: Dashed lines: simulations using DMfit[62] and the NMR parameters given in Table 2 (site 1, in green, site 2, in purple; sum: red solid line). Black solid line: experimental spectrum. Vertical grey arrows: spinning sidebands of the central transitions (CT). Insert: the simulated red line (sum of site 1 + site 2) corresponds to CT broadened by second-order quadrupolar effects *only* (see main text). **(B)**: Dashed lines: simulations using the NMR parameters given in Table 2 (site 1, in green, site 2, in purple; sum: red solid line). Black solid line: experimental spectrum. Isotropic parts and spinning sidebands (SSBs) of the CT are superimposed here. **(C)**: Dashed lines: simulations using the NMR parameters given in Table 2 (site 1, in green, site 2, in purple; sum: red solid line). Black solid line: experimental spectrum. Vertical grey arrows: spinning sidebands of the central transitions (CT). See Table S1 for NMR parameters.

In contrast with the difficulty resolving the three different Nb sites found in $K_8Nb_6O_{19},16H_2O$,[54] the spectra obtained for $Na_7HNb_6O_{19},15H_2O$ (**1**) could be reasonably simulated by using two distinct lineshapes broadened by second-order quadrupolar *and* CSA effects. The starting values for the NMR parameters were first determined using the spectrum exhibiting the most significant

discontinuities (*i.e.* $\nu_{rot}$ = 65 kHz, 700 MHz, see Figure 4 (A)). As CSA and second-order quadrupolar effects have an opposite dependence on $B_0$, the parameters were further refined at higher field (850 MHz) (Figure 4 (C)) (and also by varying $\nu_{rot}$ – see Figure 4 (B)). The optimized $^{93}$Nb NMR parameters were all derived from echo MAS NMR experiments are presented in Table 2. These results confirmed the previously reported crystallographic structure determined by single crystal X-ray diffraction studies,[20] as two groups of Nb atoms are indeed expected (protonated sites, $NbO_5O_{\mu 2}H$, and non-protonated sites, $NbO_6$).

**Table 2:** $^{93}$Nb NMR parameters determined for $Na_7HNb_6O_{19},15H_2O$. (1). See also Figure 4. Parameters were extracted by using DMfit[62] and simulations at variable magnetic field and $\nu_{rot}$ and under static mode (see Figure S9). The definitions of all parameters are given in the Experimental section. Site 1: $NbO_5O_{\mu 2}H$. Site 2: $NbO_6$ (based of integration of the lines – see main text).

| | $\delta_{iso}$ (± 10 ppm) | $C_Q$ (± 0.5 MHz) | $\eta_Q$ (± 0.1) | $\delta_{CSA}$ (± 15 ppm) | $\eta_{CSA}$ (± 0.05) | {φ°,χ°,Ψ°} | Integration (%) |
|---|---|---|---|---|---|---|---|
| **Site 1** | – 890 | 35.0 | 0.3 | + 550 | 0.95 | {0°± 5°,42± 2°, – 20°± 5°} | ~ 34 |
| **Site 2** | – 880 | 56.5 | 0.9 | + 650 | 0.95 | {105°± 3°,78°± 2°,26°± 6°} | ~ 66 |

Several comments can be made on the simulations presented in Figure 4: *(i)* the extracted $\delta_{iso}$($^{93}$Nb) values are comparable for Nb sites 1 and 2, whereas they can be clearly distinguished by their respective $C_Q$ values. It follows that both sites were distinguished best at the *lowest*

magnetic field (as second-order quadrupolar effects are then dominant). We stress that the observed $\delta_{iso}(^{93}Nb)$ for **(1)** were in agreement with data already published in the literature for niobium oxides,[54,55] *(ii)* CSA effects have to be taken into account for accurate simulations. In absence of such interaction, the spinning sidebands associated to the central transitions are clearly underestimated (see the insert in Figure 4 (A)). The intensities of the first sidebands of the central transitions were very useful for the determination of $\delta_{CSA}$ and $\{\varphi,\chi,\Psi\}$ Euler angles. Again we stress the fact that the extracted $\delta_{CSA}$ values were again comparable to published data,[54,55] *(iii)* the clear separation of central transitions from the corresponding spinning sidebands is achieved at ultra-fast MAS. At moderate MAS (30 kHz – see Figure 4 (B)), all contributions are superimposed. Nevertheless, such spectra remain useful for further refinement of the parameters presented in Table 2, *(iv)* accurate integration of the lines has to take into account the central transitions *and* the associated spinning sidebands. A ratio ~ *1:2* is obtained for *site 1: site 2*. From MAS experiments, the following $^{93}Nb$ NMR parameters were extracted as first reasonable estimations: site 1, $\delta_{iso} = -890$ ppm, $\delta_{CSA} = +550$ ppm, $\eta_{CSA} = 1$, $C_Q = 33.0$ MHz, $\eta_Q = 0.3$, $\{\varphi,\chi,\Psi\} = \{0,50,-30\}$; site 2, $\delta_{iso} = -880$ ppm, $\delta_{CSA} = +650$ ppm, $\eta_{CSA} = 1$, $C_Q = 55.0$ MHz, $\eta_Q = 0.5$, $\{\varphi,\chi,\Psi\} = \{70,90,0\}$. In order to further validate $^{93}Nb$ CSA parameters and Euler angles, static experiments were performed at 16.4 T. It is indeed established that such experiments should help for an even more accurate determination of these parameters. From the NMR point of view, this can be considered as a challenge since $C_Q$ for both sites can be considered as large or very large leading to: *(i)* a strong broadening of the static lineshapes and *(ii)* a dramatic decrease of the signal to noise ratio. In order to circumvent this particular problem, the WURST QCPMG[57] approach was implemented successfully. The efficiency of the WURST excitation was carefully checked by variable offset experiments. It was clearly

demonstrated that a *single* offset experiment was sufficient to obtain an undistorted lineshape for (**1**). Indeed, variations of the offset (±150 kHz) showed no significant variations of the global spikelet intensities. The $^{93}$Nb WURST QCPMG spectra of (**1**) and commercial $NaNbO_3$ are presented in Figure S9. $NaNbO_3$ was used here as a reference compound with $C_Q \sim 20$ MHz.[55] The corresponding simulation obtained by using parameters already published by Hanna *et al.*[55] is in very good agreement with the envelope of the spikelets. The spectrum of (**1**) is characterized by a broad and complex lineshape. Nevertheless, it exhibits clear discontinuities which are related to the subtle interplay between CSA and quadrupolar tensors (through Euler angles for both sites 1 and 2). Despite the intrinsic complexity of the spectrum, a two-site simulation could be safely derived starting from the data derived from MAS experiments (see above). Most importantly, it was demonstrated that the final lineshape was highly sensitive to small variations of the NMR parameters. As a representative example, the strong influence of the Euler angle $\chi^{(\circ)}$ for site 1 is presented in Figure S9. It follows that accurate NMR parameters could be finally extracted for sites 1 and 2: they are summarized in Table 2.

In contrast to $K_8Nb_6O_{19},16H_2O$ (**2**), $Na_7HNb_6O_{19},15H_2O$ (**1**) exhibits one proton bound to one bridging oxygen (Nb-OH-Nb) (Figure 1). This yields a unique situation where Nb atoms in the $Nb_6O_{19}$ moiety have readily two different environments. Indeed, when the $Nb_6O_{19}$ cluster is fully deprotonated, there are only minor differences between the Nb sites which renders their NMR signatures very difficult to distinguish, as already reported for $K_8Nb_6O_{19},16H_2O$ (**2**).[54] Similarly, if more than one proton is bound to $Nb_6O_{19}$, several isomers could be formed which would render the NMR study more complex. The $^{93}$Nb chemical shifts observed for (**1**) are in the range of what is expected for the distorted $NbO_6$ and $NbO_5O_{\mu 2}H$ octahedra. For comparison, the $\delta_{iso}(^{93}Nb)$ reported[54] for $K_8Nb_6O_{19},16H_2O$ range from −772 to −920 ppm (including here

experimental and *ab initio* computed parameters). As already stated above, $\delta_{iso}(^{93}Nb)$ was not able to distinguish $NbO_6$ from $NbO_5O_{\mu 2}H$ sites. However, $C_Q(^{93}Nb)$ parameters allowed an assignment for niobium sites 1 and 2 to be proposed based on point *(iv)* (see above). Following the ~ *1:2* ratio, the line with the smaller $C_Q(^{93}Nb)$ (33.0 MHz – see Table 2) was assigned to $NbO_5O_{\mu 2}H$ (2 sites *per* $Nb_6O_{19}$ cluster) whereas the larger $C_Q(^{93}Nb)$ (55.0 MHz) is assigned to $NbO_6$ (4 sites *per* $Nb_6O_{19}$ cluster). We stress here that the *Pmnn* space group for **(1)**[20] led to the presence of four $NbO_5O_{\mu 2}H$ sites *per* $Nb_6O_{19}$ cluster due to symmetry operations but *only two* of them were present from the stoichiometric point of view. It follows that some distribution should be expected for the chemical environment of the Nb atoms. Such distributions were clearly not detected by $^{93}Nb$ MAS NMR, as only two sets of NMR parameters were indeed sufficient for the accurate description of the spectra (Table 2). This point is also discussed in the context of the $^{23}Na$ MAS and 3QMAS NMR data. We close this section by mentioning that some authors have applied the concept of local distortion around a given quadrupolar nucleus in order to interpret the magnitude of $C_Q$.[72,73] Such distortions are characterized by the so-called strain ($|\Psi|$) and longitudinal strain ($|\alpha|$) parameters (calculated from experimental bond angles and bond lengths). Unfortunately, Hanna *et al.*[55] demonstrated very nicely that no clear correlation could be established between $|\Psi|$ and/or $|\alpha|$ and $C_Q(^{93}Nb)$. In other words, such an approach did not allow for the assignment of $Nb_5OH$ and $NbO_6$ sites based on the effects of local geometry on $C_Q(^{93}Nb)$.

**$^{23}$Na MAS NMR.**

As a result of its natural abundance (100%), $^{23}Na$ (I = 3/2) is a very amenable nucleus for NMR study, so that $^{23}Na$ MAS NMR has proven to be an efficient tool to characterize

polyoxometalates such as $Na_6P_2Mo_5O_{23},7H_2O$ or $Na_{15}(PO_2)_3PNb_9O_{34},22H_2O$.[41,74] Nonetheless, $^{23}Na$ NMR has never been used to investigate hexaniobate or hexatantalate salts (to the best of our knowledge). Here we probed $Na_7HNb_6O_{19},15H_2O$ (**1**) and $Na_8Ta_6O_{19},24.5H_2O$ (**3**) by $^{23}Na$ solid state 1D MAS and 3Q MAS NMR**.**

The 1D and 2D $^{23}Na$ NMR spectra of (**1**) are given in Figure 5. Fast MAS at 40 kHz led to a very well resolved spectrum exhibiting several overlapping resonances. We stress here that by increasing $\nu_{rot}$ up to 65 kHz, small continuous variations of some $\delta_{iso}(^{23}Na)$ (< 0.3 ppm) were observed. Such variations were fully *reversible* by lowering $\nu_{rot}$ and could be interpreted in terms of local heating of the sample due to friction of the rotor at the highest rotation frequencies.

The 1D $^{23}Na$ fast MAS spectrum was simulated by using information extracted from the 3QMAS experiment (see the insert in Figure 5 and Table 3). In order to quantify the various isotropic resonances, the contribution of the isotropic part of the satellite transitions was taken into account (see the Experimental section and peak #7 in Figure 5). Five main peaks with an average intensity of ~ 18 % (max. 25 %; min. 12 %) could be observed with significant variations of $C_Q(^{23}Na)$. For three of the peaks (#4,5,6 in Figure 5), the quadrupolar interaction was considered as negligible and Lorentz/Gauss lineshapes were used for the simulations.

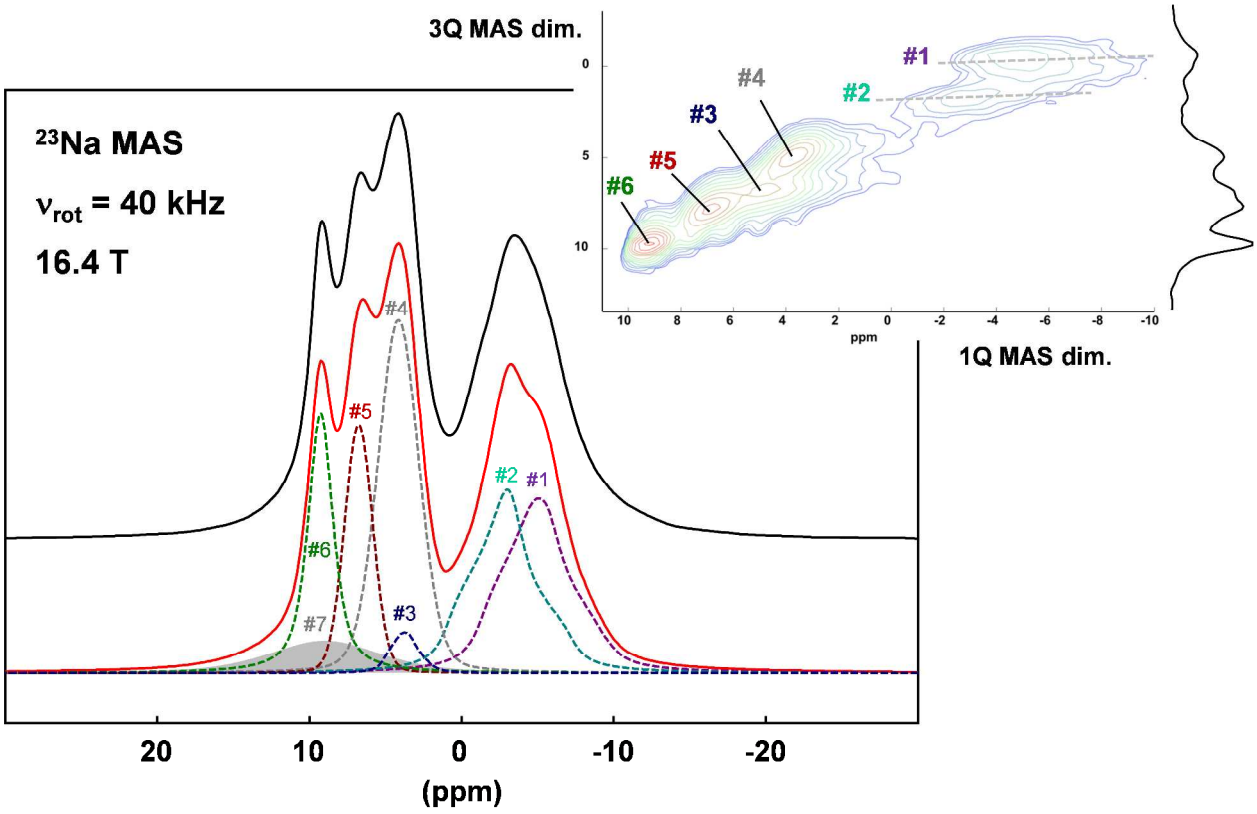


**Figure 5:** $^{23}$Na MAS NMR spectrum of $Na_7HNb_6O_{19},15H_2O$ **(1)**. Insert: $^{23}$Na 3QMAS NMR spectrum. The simulated NMR parameters for #1 to #7 are given in Table 3. See Table S1 for NMR parameters.

**Table 3:** $^{23}$Na NMR parameters determined for $Na_7HNb_6O_{19},15H_2O$. (1). See also Figure 5. Parameters were extracted by using DMfit.[62] The definitions of all parameters are given in the Experimental section. The various peaks are labeled # (see Figure 5). #1 to #3: second-order quadrupolar broadened lineshapes (central transitions). #4 to #6: Lorentz/Gauss lineshapes. #7: isotropic contribution of the satellites transitions.

| site # | $\delta_{iso}$ (± 0.15 ppm for #1 to #3 ) (± 0.08 ppm for #4 to #6 ) | $C_Q$ (± 0.05 MHz) | $\eta_Q$ (± 0.10) | Integration (%) |
|---|---|---|---|---|
| **#1** | – 1.30 | 2.07 | 0.75 | 21 |
| **#2** | + 0.90 | 1.95 | 0.90 | 19 |
| **#3** | + 5.20 | 1.32 | 0.60 | ~ 2 |
| **#4** | + 4.20 | < 0.03 | - | 25 |
| **#5** | + 6.80 | < 0.03 | - | 12 |
| **#6** | + 9.30 | < 0.03 | - | 14 |
| **#7** | +9.00 | - | - | 7 |

The crystal structure of $Na_7HNb_6O_{19},15H_2O$ **(1)**, determined at 173 K by Anderson et al.,[20] exhibits only *four* distinct sodium sites in the asymmetric unit (see Table S2). It follows that an apparent contradiction exists between expectations from the crystallography and the experimental number of isotropic $^{23}$Na peaks observed at near room temperature (~ 318 K). One must remember that some disorder due to the presence of a *unique* $NbO_5O_{\mu 2}H$ site in the hexaniobate cluster must be considered to fully analyze the NMR spectra (see also the $^{93}$Nb MAS section above). Such local disorder from one cluster to the other could explain the higher multiplicity of the $^{23}$Na sites. Looking carefully at Figure 5, a sixth component (peak #3) could be extracted from the 2D 3QMAS experiment. The intensity of this particular peak derived from the 1D $^{23}$Na spectrum is very small (~ 2 %). We make the reasonable assumption that this peak corresponds to an impurity. Indeed, even though special care was taken to remove the excess of NaOH necessary for the synthesis of (**1**), it could not be ruled out that the appearance of the sixth sodium site in the MAS NMR spectrum of (**1**) resulted from the presence of a small proportion

of fully deprotonated clusters $Na_8Nb_6O_{19},15H_2O$. This highlights the difficulty of isolating pure hexaniobate salts and that multiple techniques are needed to discriminate between the numerous phases that can be formed (Table 1). No attempts were made to further assign the five major $^{23}Na$ resonances to particular Na sites in the structure of **(1)** nor to correlate the variations of $C_Q(^{23}Na)$ with the local chemical environment of sodium sites as it would necessitate the *ab initio* calculations of $^{23}Na$ parameters using supercells to take disorder into account.[54,75] Such a work is outside the scope of this contribution.

In our attempt to further characterize polyoxometalates by NMR, we also probed $Na_8Ta_6O_{19},24.5H_2O$ (**3**) by $^{23}Na$ MAS NMR. The spectrum of (**3**) recorded at 16.4 T and 30 kHz displayed a very complicated spectrum (Figure 6) which involved most probably a superposition of Na sites with variable $C_Q$. Importantly, the $^{23}Na$ chemical shifts observed for (**3**) were in the same range as for the hexaniobate salt (**1**) indicating that $Ta_6O_{19}/Nb_6O_{19}$ clusters and water molecules have a similar effect on Na. The crystal structure of (**3**) was recently resolved by Abramov *et al.*[17] and displays a layered structure with 10 non-equivalent sodium sites in the asymmetric unit. It follows that the analysis of the corresponding $^{23}Na$ MAS NMR spectrum should imply at least 10 non-equivalent contributions (if XRD data are strictly followed and that no disorder is present). In order to further characterize (**3**), $^{23}Na$ 3Q MQ MAS experiment was performed (Figure S10). Such an experiment led to a partial disentanglement of the corresponding $^{23}Na$ MAS spectrum. Indeed, two well-defined peaks were identified. The first one is characterized by $\delta_{iso}$ = + 0.50 ppm, $C_Q$ = 1.80 MHz (assuming here $\eta_Q$ = 1). The second one centered at $\delta_{iso}$ = + 6.35 ppm is not subjected to any measurable quadrupolar interaction (LW = 215 Hz). Most interestingly, a much less defined component was evidenced as well. It remained difficult to characterize it more precisely due to the eventual presence of distributions

of NMR parameters. In other words, X-ray diffraction data showing 10 non-equivalent sites (see above) could maybe correspond to an average structure (exhibiting more structural complexity at the *local* NMR level).

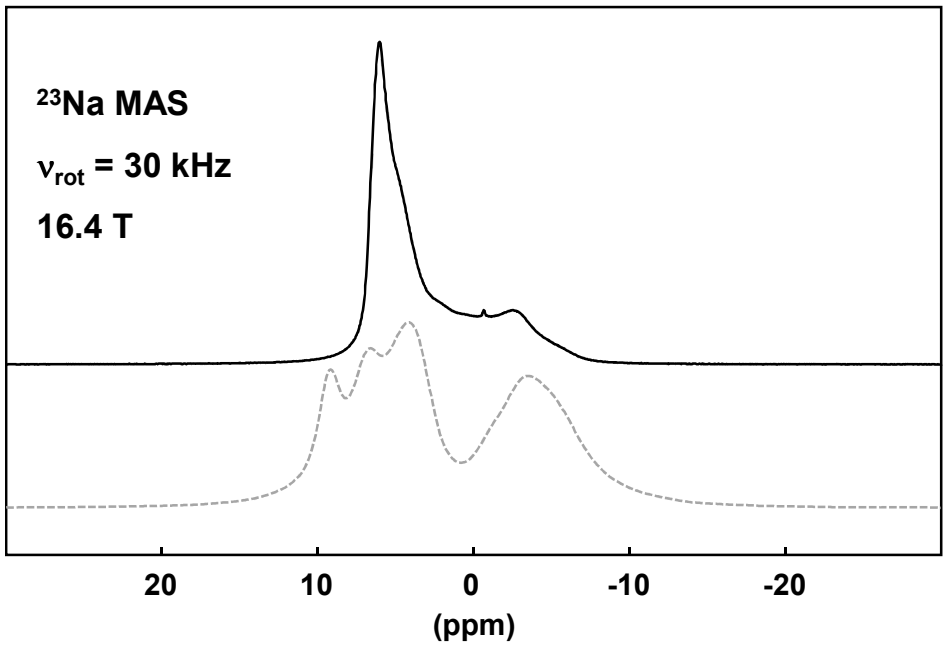


**Figure 6:** Solid line: $^{23}$Na MAS NMR spectra of $Na_8Ta_6O_{19},24.5H_2O$ **(3)**. Dashed line: $^{23}$Na MAS NMR spectrum of $Na_7HNb_6O_{19},15H_2O$ **(1)** for comparison. See Table S1 for NMR parameters.

**Study of Ta doped $Na_7HNb_6O_{19},15H_2O$.**

Finally, the Nb-Ta substitution in the cluster $M_6O_{19}$ was investigated by solid state MAS NMR. The synthesis of $Na_7HNb_6O_{19},15H_2O$ **(1)** was performed by alkaline fusion, as described in the Experimental Section, but $Ta_2O_5$ was added to the starting material ($Nb_2O_5$) before the synthesis. The Nb/Ta ratio used for the study was 17.4/1 which corresponds to the formula $Na_7HNb_{5.67}Ta_{0.33}O_{19},15H_2O$, or in other words, one atom of tantalum for three $M_6O_{19}$ clusters.

The substitution of niobium by tantalum in the cluster $Nb_6O_{19}$ did not significantly influence the $^{93}$Nb echo MAS NMR spectra (see insert (A) in Figure 7). Only a very slight smoothing of the discontinuities was observed. The lack of distinguishing the different sites is thought to be due to the intrinsic low resolution of $^{93}$Na MAS NMR and most probably the low Ta doping rate used in the study. Moreover, the crystallographic structure of (**1**) is not expected to change significantly (as checked by powder XRD; data not shown) due to the low tantalum doping, and due to the identical ionic radius of Ta(V) and Nb(V) (*i.e.* 64 pm if CN = 6). On the other hand, $^{23}$Na MAS NMR was found to be more sensitive at following the Nb/Ta substitution in $Na_7HNb_6O_{19},15H_2O$ (**1**) (Figure 7). When (**1**) was doped with tantalum, the $^{23}$Na MAS spectrum was clearly modified. The modification of the spectrum was further characterized by $^{23}$Na 3Q MAS experiment (Figure S11). The importance of a peak at $\delta_{iso}$ = 4.75 ppm, $C_Q$ = 2.31 MHz and $\eta_Q$ = 0.78 was clearly evidenced. This corresponds to the main difference between (**1**) and the Ta doped structure. The complete simulation of the $^{23}$Na MAS spectrum (with relative integrations) is also given in Figure S11. A direct comparison can be established with data obtained for (**1**) (see Table 3). The complexity of the spectrum increases with Ta doping in agreement with the expected increase of structural disorder in the doped structure.

One realistic structural assumption is to suppose that the insertion of tantalum in $Na_7HNb_6O_{19},15H_2O$ (**1**) induced a partial substitution of the proton, linked to the cluster, by a sodium ion leading to the general formula $Na_{7+y}H_{1-y}Nb_{5.67}Ta_{0.33}O_{19},15H_2O$. Such an assumption was confirmed by $^1$H solid state MAS NMR. The insert (B) in Figure 7 gives the comparison between the $^1$H NMR spectra of (**1**) and the Ta-doped sample. The broad peak at + 6.3 ppm due to the water molecules and the much less intense peak at +1.9 ppm due to the $NbO_5O_{\mu 2}H$ sites of the clusters in (**1**) were still observed but an additional sharp peak appeared at ~ + 4.9 ppm. This

value is strictly comparable to those observed in Figure 3. As discussed for $K_8Nb_6O_{19},16H_2O$ (**2**) and $Na_8Ta_6O_{19},24.5H_2O$ (**3**) (see the $^1H$ NMR section above), the water molecules surrounding a fully deprotonated cluster exhibit a rather sharp (but composite) $^1H$ NMR resonance (see Figure 3). This means that, when the Nb/Ta substitutions took place, fully deprotonated clusters were formed, supporting the $^{23}Na$ NMR observations. A quantitative analysis of the loss of $NbO_5O_{\mu 2}H$ sites upon substitution by Ta was not performed here due to the complexity of the broad water resonance (see above).

The study of several deprotonated $Nb_6O_{19}$ and $Ta_6O_{19}$ structures, performed by Anderson *et al.,*[20] revealed that the Ta-clusters have slightly longer M=O bonds than their Nb counterparts. For example, the average M=O distances in $Na_7HNb_6O_{19},15H_2O$ (**1**) and the isostructural $Na_8Ta_6O_{19},15H_2O$ (**3**) are 1.770 and 1.799 ± 0.003Å, respectively. In the crystal of (**1**), the $NbO_5O_{\mu 2}H$ site has also the longest Nb=O bond length (1.780 *vs* 1.760 Å), respectively. Therefore this site is more prone to accommodate the Nb-Ta substitution. This assumption was clearly corroborated by $^1H$ MAS NMR data (insert (B) in Figure 7) where the resonance at ~ + 4.9 ppm can be safely related to deprotonated clusters. Since (**1**) was synthesized by alkaline fusion at high temperature (450 °C), Ta was initially expected to be homogenously distributed.[76] However, as the ~ + 4.9 ppm resonance is clearly observed in the $^1H$ MAS spectra, the following assumption can be proposed: the Ta atoms could be incorporated in *adjacent* clusters, leading to rather isolated groups of deprotonated entities surrounded by water molecules characterized by the rather sharp resonances at ~ + 4.9 ppm. The example given here shows that the mixed metal clusters can shed light on the differences between Nb and Ta chemistries. Moreover, ones could take advantage of these differences and tune the physicochemical properties of hexametalate salts by preparing mixed Nb/Ta hexametalate salts. Obviously, multinuclear solid state NMR

appears as a highly pertinent tool for providing accurate structural details on the mixed Nb/Ta clusters.

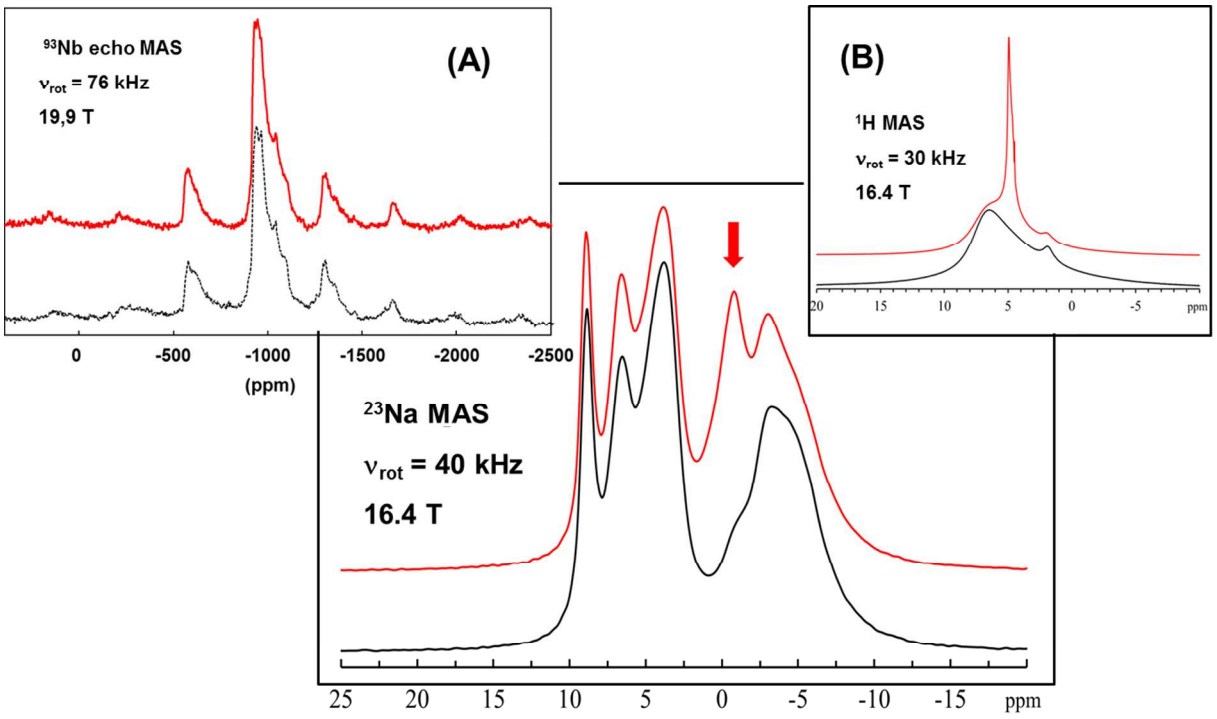


**Figure 7:** $^{23}$Na MAS NMR of $Na_7HNb_6O_{19},15H_2O$ **(1)** in black and $Na_7HNb_{5.67}Ta_{0.33}O_{19},15H_2O$ in red. The vertical red arrow stresses on the differences between both spectra. Insert (**A**): $^{93}$Nb echo MAS NMR spectra of $Na_7HNb_6O_{19},15H_2O$ **(1)** (black line) and $Na_7HNb_{5.67}Ta_{0.33}O_{19},15H_2O$ (red line). Insert (**B**): $^{1}$H MAS NMR spectra of $Na_7HNb_6O_{19},15H_2O$ (**1**) in black and $Na_7HNb_{5.67}Ta_{0.33}O_{19},15H_2O$ in red. See Table S1 for NMR parameters.

## CONCLUSION AND PERSPECTIVES

This work highlights the potential of multinuclear MAS NMR techniques to study hexaniobate and hexatantalate salts. The studies of $Na_7HNb_6O_{19},15H_2O$ (**1**), $K_8Nb_6O_{19},16H_2O$ (**2**) and $Na_8Ta_6O_{19},24.5H_2O$ (**3**) showed that *protonated* and *deprotonated* clusters were easily discriminated by $^{1}$H fast MAS and echo NMR. Moreover, we demonstrated that partial Nb/Ta substitution could be easily followed by $^{1}$H MAS NMR, as local dynamics of the water

molecules at room temperature were shown to be strongly different from protonated to deprotonated clusters. Variable temperature $^{1}$H MAS NMR experiments will be performed in a near future in order to further investigate the local motion of the water molecules. $^{93}$Nb echo MAS NMR spectra were recorded at ultra-high field and ultra-fast MAS (variable field and MAS frequency). It appeared that $NbO_5O_{\mu 2}H$ and $NbO_6$ were clearly distinguished based on variations of $C_Q(^{93}Nb)$ and relative intensities of the resonance lines. Cross Polarization (CP) from $^{1}$H to $^{93}$Nb, as well as 2D $^{1}$H-$^{1}$H correlation experiments, could be interesting options to further characterize the protonated $NbO_5O_{\mu 2}H$ sites through spectral editing. Static $^{93}$Nb spectra could be recorded (wideline NMR spectroscopy)[55] under BRAIN (broadband adiabatic inversion pulses) CP transfer.[77] Such a sequence is indeed well adapted for CP dealing with "strong" quadrupolar nuclei (high $C_Q(^{93}Nb)$ values). Work is currently in progress in the laboratory.

The $^{23}$Na MAS and 3QMAS NMR study of (**1**) revealed several sodium sites and confirmed the presence of disorder due to the presence of a unique $NbO_5O_{\mu 2}H$ site *per* cluster. The high resolution observed in $^{23}$Na MAS NMR should allow the set-up of 2D homonuclear dipolar ($^{23}$Na-$^{23}$Na) experiments in order to correlate the $^{23}$Na nuclei.[78] This approach could be of high interest for accurate analysis in the case of mixtures of hexaniobates/tantalates clusters, as $^{23}$Na NMR is sensitive to the chemical nature of the clusters. Very interestingly, the Nb/Ta substitution in (**1**) was found to be easier to follow by $^{23}$Na and $^{1}$H MAS NMR than by $^{93}$Nb MAS NMR due to the exchange between the protons linked to the cluster and sodium ion. Finally, we mention that $^{181}$Ta (I = 7/2) could be another local probe of investigation but it can be considered to be a "very strong" quadrupolar nucleus.[79]

## ASSOCIATED CONTENT

**Supporting Information**. SEM images, Raman spectra and TGA analyses of (**1**), (**2**) and (**3**). $^{93}$Nb static WURST QCPMG spectra of $NaNbO_3$ and (**1**). $^{23}$Na 3Q MAS spectra of (**2**) and (**3**). Summary of NMR parameters used in this study and crystal structure information for (**1**), (**2**) and (**3**).

## AUTHOR INFORMATION

### Corresponding Author

*E-mail: gauthier.deblonde@chimie-paris.org

## ACKNOWLEDGMENT

We authors thank Dr. Marie-Noëlle Rager (Chimie ParisTech) for helpful discussions. This work was supported by Eramet Research (France). The French Région Ile de France SESAME program is acknowledged for financial support (700 MHz spectrometer). The UK 850 MHz solid-state NMR Facility used in this research was funded by EPSRC and BBSRC, as well as the University of Warwick including *via* part funding through Birmingham Science City Advanced Materials Projects 1 and 2 supported by Advantage West Midlands (AWM) and the European Regional Development Fund (ERDF).

## REFERENCES


(1) Roskill Information Services. *The economics of niobium.*; Roskill Information Services: London, 2009.
(2) Nete, M.; Purcell, W.; Nel, J. T. *Hydrometallurgy* **2014**, *149*, 31–40.
(3) Agulyanski, A. *The chemistry of tantalum and niobium fluoride compounds*, 1st ed.; Elsevier: Amsterdam ; Boston, 2004.
(4) Deblonde, G. J.-P.; Chagnes, A.; Weigel, V.; Cote, G. *Hydrometallurgy* **2016**. In Press. DOI: 10.1016/j.hydromet.2015.12.009.
(5) Deblonde, G. J.-P.; Weigel, V.; Bellier, Q.; Houdard, R.; Delvallée, F.; Bélair, S.; Beltrami, D. *Sep. Purif. Technol.* **2016**, *162*, 180–187.
(6) Wang, X.; Zheng, S.; Xu, H.; Zhang, Y. *Hydrometallurgy* **2009**, *98*, 219–223.
(7) Marignac, M. C. *Ann. Chim. Phys.* **1866**, *8*, 5–75.
(8) Nyman, M. *Dalton Trans.* **2011**, *40*, 8049–8058.
(9) Deblonde, G. J.-P.; Moncomble, A.; Cote, G.; Bélair, S.; Chagnes, A. *RSC Adv.* **2015**, *5*, 7619–7627.
(10) Deblonde, G. J.-P.; Delaunay, N.; Lee, D.; Chagnes, A.; Cote, G. *RSC Adv.* **2015**, *5*, 64119–64124.
(11) Lindqvist, I. *Ark. För Kemi* **1953**, *5*, 247–250.
(12) Zhou, H.; Zheng, S.; Zhang, Y. *Hydrometallurgy* **2005**, *80*, 83–89.
(13) Zhou, H.; Zheng, S.; Zhang, Y.; Yi, D. *Hydrometallurgy* **2005**, *80*, 170–178.
(14) Nyman, M.; Anderson, T. M.; Provencio, P. P. *Cryst. Growth Des.* **2009**, *9*, 1036–1040.
(15) Shen, L.; Xu, Y.-Q.; Gao, Y.-Z.; Cui, F.-Y.; Hu, C.-W. *J. Mol. Struct.* **2009**, *934*, 37–43.
(16) Britvin, S. N.; Siidra, O. I.; Lotnyk, A.; Kienle, L.; Krivovichev, S. V.; Depmeier, W. *Inorg. Chem. Commun.* **2012**, *25*, 18–20.
(17) Abramov, P. A.; Abramova, A. M.; Peresypkina, E. V.; Gushchin, A. L.; Adonin, S. A.; Sokolov, M. N. *J. Struct. Chem.* **2011**, *52*, 1012–1017.
(18) Deblonde, G. J.-P.; Chagnes, A.; Bélair, S.; Cote, G. *Hydrometallurgy* **2015**, *156*, 99–106.
(19) Muller, M. *Rev. Chim. Minérale* **1970**, *7*, 359.
(20) Anderson, T. M.; Rodriguez, M. A.; Bonhomme, F.; Bixler, J. N.; Alam, T. M.; Nyman, M. *Dalton Trans.* **2007**, *40*, 4517–4522.
(21) Pickhard, F.; Hartl, H. *Z. Für Anorg. Allg. Chem.* **1997**, *623*, 1311–1316.
(22) Balogh, E.; Anderson, T. M.; Rustad, J. R.; Nyman, M.; Casey, W. H. *Inorg. Chem.* **2007**, *46*, 7032–7039.
(23) Sahureka, F.; Burns, R. C.; von Nagy-Felsobuki, E. I. *Inorganica Chim. Acta* **2003**, *351*, 69–78.
(24) Matsumoto, M.; Ozawa, Y.; Yagasaki, A. *Inorg. Chem. Commun.* **2011**, *14*, 115–117.
(25) Filowitz, M.; Ho, R. K. C.; Klemperer, W. G.; Shum, W. *Inorg. Chem.* **1979**, *18*, 93–103.
(26) Besserguenev, A. V.; Dickman, M. H.; Pope, M. T. *Inorg. Chem.* **2001**, *40*, 2582–2586.
(27) Nelson, H. W.; Tobias, S. *Inorg. Chem.* **1963**, *2*, 985–992.
(28) Farrell, F. J.; Maroni, V. A.; Spiro, T. G. *Inorg. Chem.* **1969**, *8*, 2638–2642.
(29) Aveston, J.; Johnson, J. S. *Inorg. Chem.* **1964**, *3*, 1051–1053.
(30) Dehand, J. *Rev. Chim. Minérale* **1965**, *2*, 259–293.
(31) Hartl, H.; Pickhard, F.; Emmerling, F.; Röhr, C. *Z. Für Anorg. Allg. Chem.* **2001**, *627*, 2630–2638.
(32) Matsumoto, M.; Ozawa, Y.; Yagasaki, A. *Inorg. Chem.* **2012**, *51*, 5991–5993.

(33) Matsumoto, M.; Ozawa, Y.; Yagasaki, A.; Zhe, Y. *Inorg. Chem.* **2013**, *52*, 7825–7827.
(34) Hou, Y.; Fast, D. B.; Ruther, R. E.; Amador, J. M.; Fullmer, L. B.; Decker, S. R.; Zakharov, L. N.; Dolgos, M. R.; Nyman, M. *J. Solid State Chem.* **2015**, *221*, 418–425.
(35) Flynn Jr, C. M.; Stucky, G. D. *Inorg. Chem.* **1969**, *8*, 332–334.
(36) Alam, T. M.; Nyman, M.; Cherry, B. R.; Segall, J. M.; Lybarger, L. E. *J. Am. Chem. Soc.* **2004**, *126*, 5610–5620.
(37) Tong, H.; Ye, J. *Eur. J. Inorg. Chem.* **2010**, 1473–1480.
(38) Niu, J.; Ma, P.; Niu, H.; Li, J.; Zhao, J.; Song, Y.; Wang, J. *Chem. - Eur. J.* **2007**, *13*, 8739–8748.
(39) Bonhomme, F.; Larentzos, J. P.; Alam, T. M.; Maginn, E. J.; Nyman, M. *Inorg. Chem.* **2005**, *44*, 1774–1785.
(40) Goiffon, A.; Philippot, E.; Maurin, E. *Rev. Chim. Minérale* **1980**, *17*, 466–476.
(41) Nyman, M.; Celestian, A. J.; Parise, J. B.; Holland, G. P.; Alam, T. M. *Inorg. Chem.* **2006**, *45*, 1043–1052.
(42) Kinomura, N.; Kumata, N.; Muto, F. *Mater. Res. Bull.* **1984**, *19*, 299–304.
(43) Kennedy, J. H. *J. Inorg. Nucl. Chem.* **1961**, *20*, 53–57.
(44) Zhang, D.; Li, S.; Wang, J.; Niu, J. *Inorg. Chem. Commun.* **2012**, *17*, 75–78.
(45) Ma, P.; Wang, G.; Chen, G.; Wang, J.; Niu, J. *J. Mol. Struct.* **2011**, *997*, 126–130.
(46) Nyman, M.; Alam, T. M.; Bonhomme, F.; Rodriguez, M. A.; Frazer, C. S.; Welk, M. E. *J. Clust. Sci.* **2006**, *17*, 197–219.
(47) Black, J. R.; Nyman, M.; Casey, W. H. *J. Am. Chem. Soc.* **2006**, *128*, 14712–14720.
(48) Neumann, G. *Acta Chem. Scand.* **1964**, *18*, 278–280.
(49) Kong, X.; Hu, D.; Wen, P.; Ishii, T.; Tanaka, Y.; Feng, Q. *Dalton Trans.* **2013**, *42*, 7699–7709.
(50) Santos, I.; Loureiro, L. H.; Silva, M. F. P.; Cavaleiro, A. *Polyhedron* **2002**, *21*, 2009–2015.
(51) Ohlin, C. A.; Villa, E. M.; Fettinger, J. C.; Casey, W. H. *Angew. Chem. Int. Ed.* **2008**, *47*, 8251–8254.
(52) Ohlin, C. A.; Villa, E. M.; Casey, W. H. *Inorganica Chim. Acta* **2009**, *362*, 1391–1392.
(53) Maekawa, M.; Ozawa, Y.; Yagasaki, A. *Inorg. Chem.* **2006**, *45*, 9608–9609.
(54) Papulovskiy, E.; Shubin, A. A.; Terskikh, V. V.; Pickard, C. J.; Lapina, O. B. *Phys. Chem. Chem. Phys.* **2013**, *15*, 5115–5131.
(55) Hanna, J. V.; Pike, K. J.; Charpentier, T.; Kemp, T. F.; Smith, M. E.; Lucier, B. E. G.; Schurko, R. W.; Cahill, L. S. *Chem. - Eur. J.* **2010**, *16*, 3222–3239.
(56) Zhou, D. H.; Hoatson, G. L.; Vold, R. L. *J. Magn. Reson.* **2004**, *167*, 242–252.
(57) Schurko, R. W. *Acc. Chem. Res.* **2013**, *46*, 1985–1995.
(58) Iuga, D.; Schäfer, H.; Verhagen, R.; Kentgens, A. P. . *J. Magn. Reson.* **2000**, *147*, 192–209.
(59) Medek, A.; Harwood, J. S.; Frydman, L. *J. Am. Chem. Soc.* **1995**, *117*, 12779–12787.
(60) Amoureux, J.-P.; Fernandez, C.; Steuernagel, S. *J. Magn. Reson. A* **1996**, *123*, 116–118.
(61) Sakellariou, D.; Lesage, A.; Hodgkinson, P.; Emsley, L. *Chem. Phys. Lett.* **2000**, *319*, 253–260.
(62) Quadrupolar + CSA Static and MAS | dmfit - D.Massiot - NMR@CEMHTI CNRS UPR3079 Orléans France http://nmr.cemhti.cnrs-orleans.fr/dmfit/help/models/QUAD_CSA.aspx (accessed Feb 9, 2016).
(63) Grey, C. P.; Vega, A. J. *J. Am. Chem. Soc.* **1995**, *117*, 8232–8242.

(64) Pourpoint, F.; Gervais, C.; Bonhomme-Coury, L.; Azaïs, T.; Coelho, C.; Mauri, F.; Alonso, B.; Babonneau, F.; Bonhomme, C. *Appl. Magn. Reson.* **2007**, *32*, 435–457.
(65) Alam, T. M.; Nyman, M.; McIntyre, S. K. *J. Phys. Chem. A* **2007**, *111*, 1792–1799.
(66) Jehng, J.-M.; Wachs, I. E. *Chem. Mater.* **1991**, *3*, 100–107.
(67) Johnston, K. E.; Griffin, J. M.; Walton, R. I.; Dawson, D. M.; Lightfoot, P.; Ashbrook, S. E. *Phys. Chem. Chem. Phys.* **2011**, *13*, 7565–7576.
(68) Yamada, K.; Shimizu, T.; Nakai, T.; Deguchi, K.; Yue, B.; Ye, J. *Chem. Lett.* **2013**, *42*, 1223–1224.
(69) Chenu, S.; Werner-Zwanziger, U.; Calahoo, C.; Zwanziger, J. W. *J. Non-Cryst. Solids* **2012**, *358*, 1795–1805.
(70) Papulovskiy, E.; Khabibulin, D. F.; Terskikh, V. V.; Paukshtis, E. A.; Bondareva, V. M.; Shubin, A. A.; Andreev, A. S.; Lapina, O. *J. Phys. Chem. C* **2015**, *119*, 10400–10411.
(71) Perić, B.; Gautier, R.; Pickard, C. J.; Bosiočić, M.; Grbić, M. S.; Požek, M. *Solid State Nucl. Magn. Reson.* **2014**, *59–60*, 20–30.
(72) Ghose, S.; Tsang, T. *Am. Mineral.* **1973**, *58*, 748–755.
(73) MacKenzie, K. J. D.; Smith, M. E. *Multinuclear Solid-State Nuclear Magnetic Resonance of Inorganic Materials*; Pergamon Materials Series; Elsevier Science, 2002; Vol. 6.
(74) Skibsted, J.; Brorson, M.; Villadsen, J.; Jakobsen, H. J. *Inorg. Chem.* **2000**, *39*, 4130–4136.
(75) Bonhomme, C.; Gervais, C.; Babonneau, F.; Coelho, C.; Pourpoint, F.; Azaïs, T.; Ashbrook, S. E.; Griffin, J. M.; Yates, J.; Mauri, F.; Pickard, C. J. *Chem. Rev.* **2012**, *112*, 5733–5779.
(76) Deblonde, G. J.-P.; Chagnes, A.; Cote, G.; Vial, J.; Rivals, I.; Delaunay, N. *J. Chromatogr. A* **2016**, *1437*, 210–218.
(77) Harris, K. J.; Lupulescu, A.; Lucier, B. E. G.; Frydman, L.; Schurko, R. W. *J. Magn. Reson.* **2012**, *224*, 38–47.
(78) Eden, M.; Frydman, L. *J. Phys. Chem. B.* **2003**, *107*, 14598–14611.
(79) Rod, S.; Borsa, F.; Van der Klink, J. J. *Phys. Rev. B* **1988**, *38*, 2267–2272.

$Na_7HNb_6O_{19},15H_2O$ (**1**), $K_8Nb_6O_{19},16H_2O$ (**2**) and $Na_8Ta_6O_{19},24.5H_2O$ (**3**) were probed by solid state Magic Angle Spinning (MAS) NMR at ultra-high magnetic fields (up to 19.9 T). $^{1}H$, 1D $^{23}Na$ MAS, 2D $^{23}Na$ 3QMAS and $^{93}Nb$ MAS NMR were found to be powerful and straightforward tools to discriminate between protonated and non-protonated clusters, to identify the $NbO_5O_{\mu 2}H$ and $NbO_6$ sites and to study the effect of Nb/Ta substitutions in these alkali hexaniobate and hexatantalate salts.

**FOR TABLE OF CONTENTS ONLY**

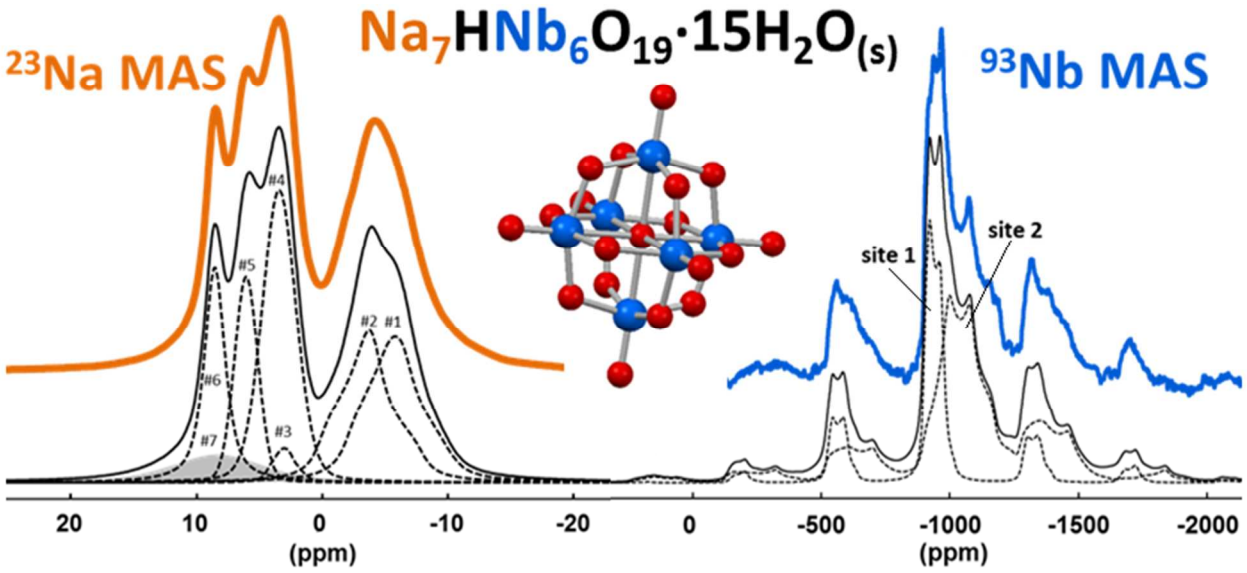

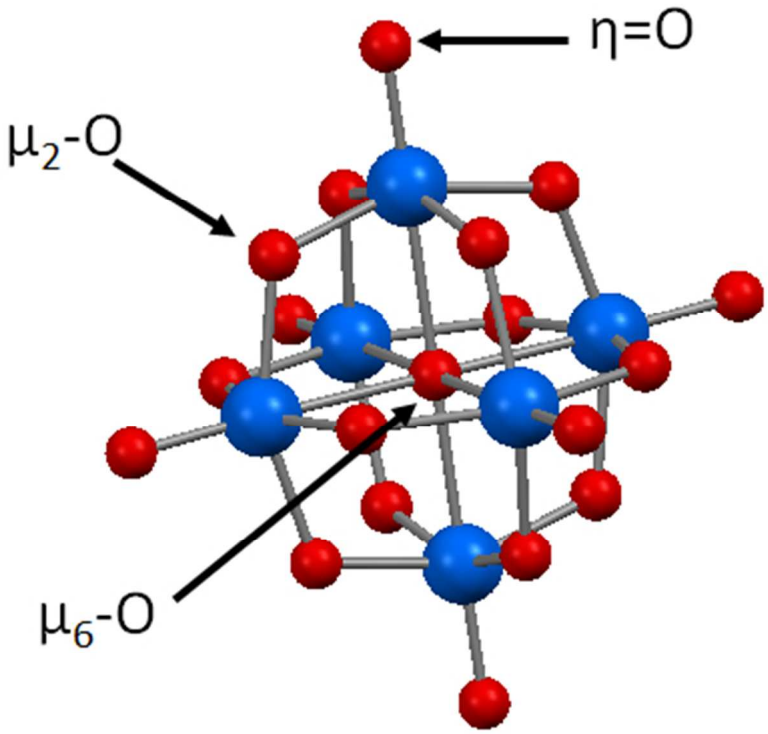


Figure 1
110x104mm (96 x 96 DPI)

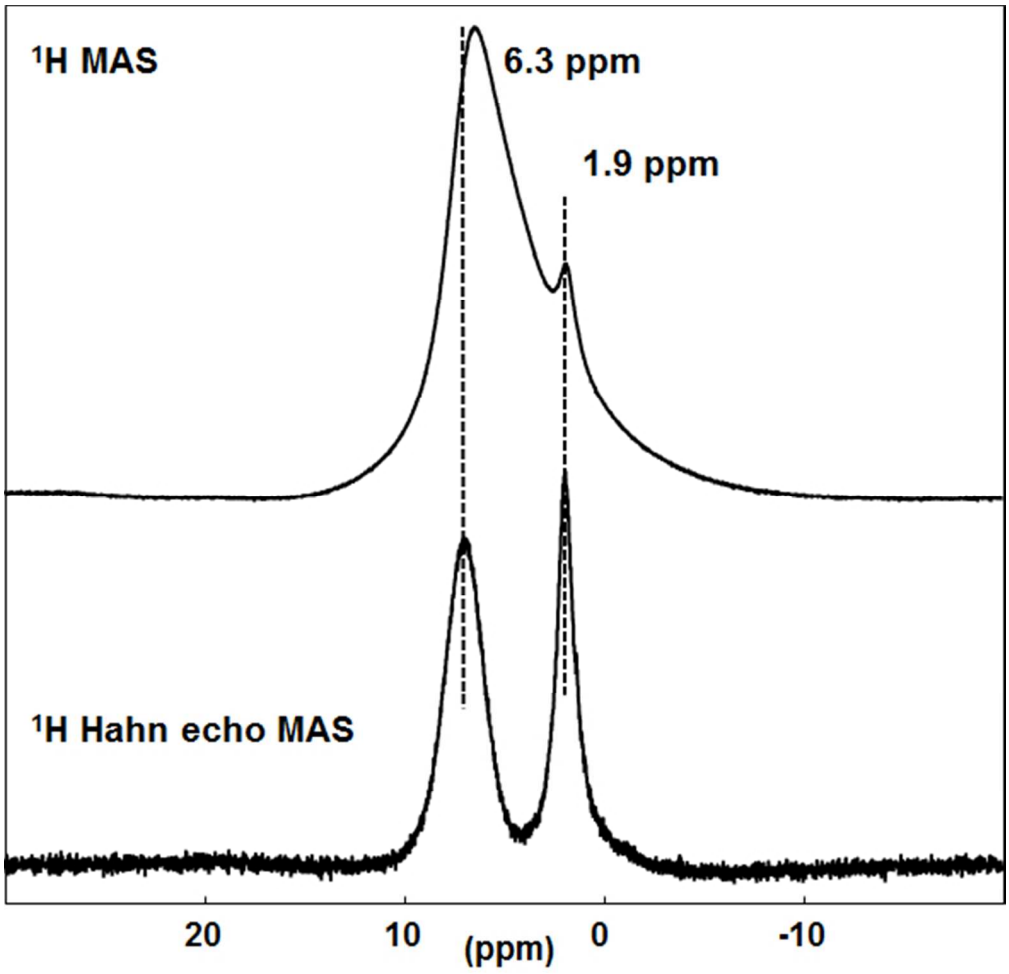


Figure 2
155x152mm (96 x 96 DPI)

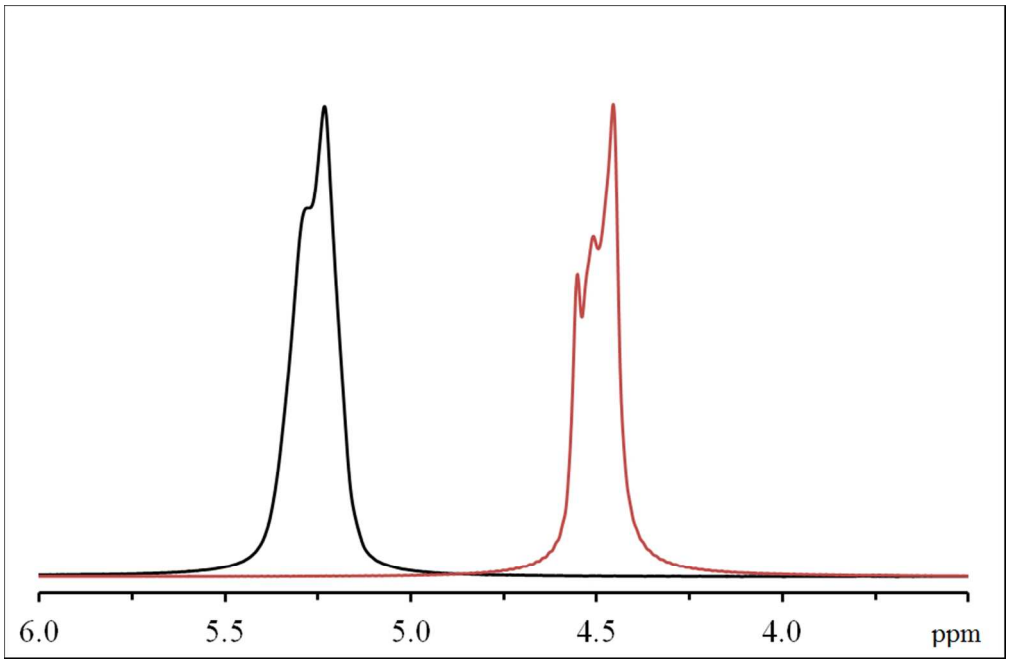


Figure 3
258x169mm (96 x 96 DPI)

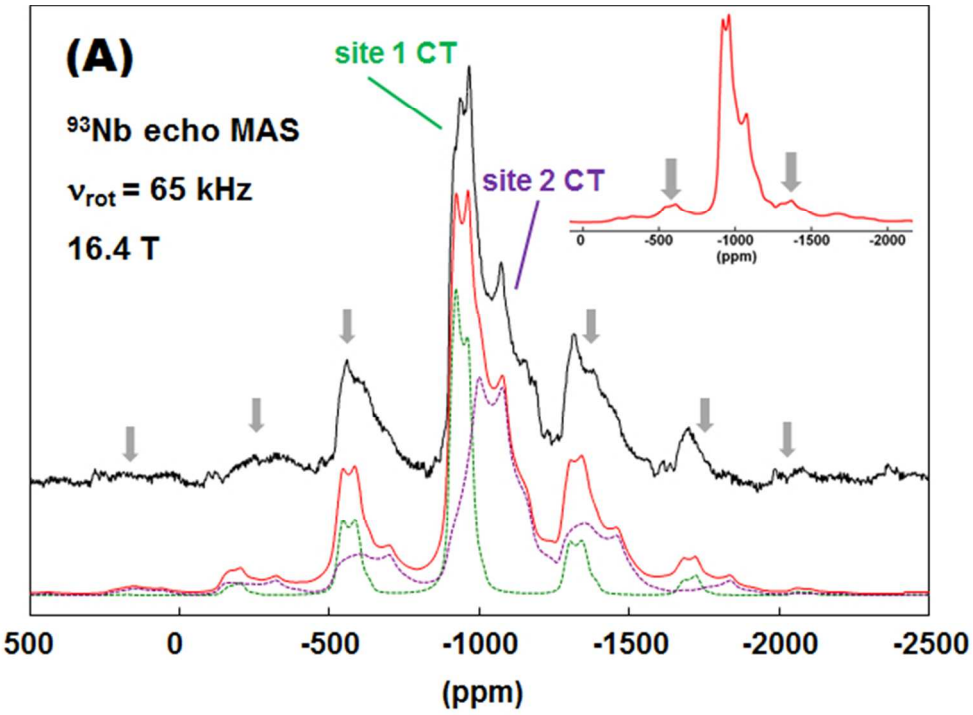


Figure 4 (A)
172x124mm (96 x 96 DPI)

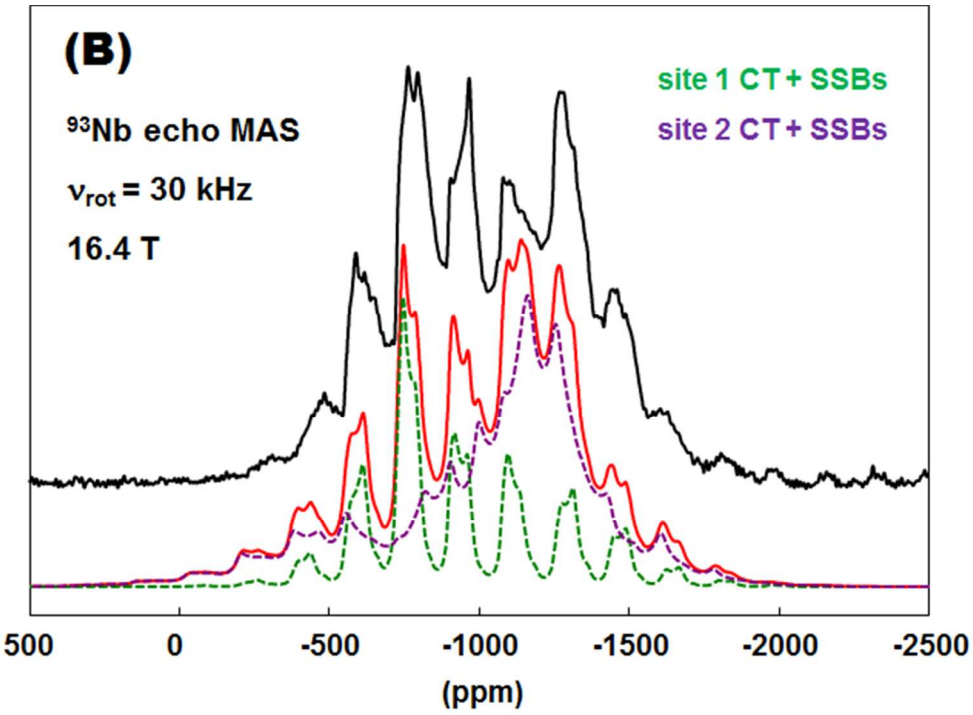


Figure 4 (B)
172x124mm (96 x 96 DPI)

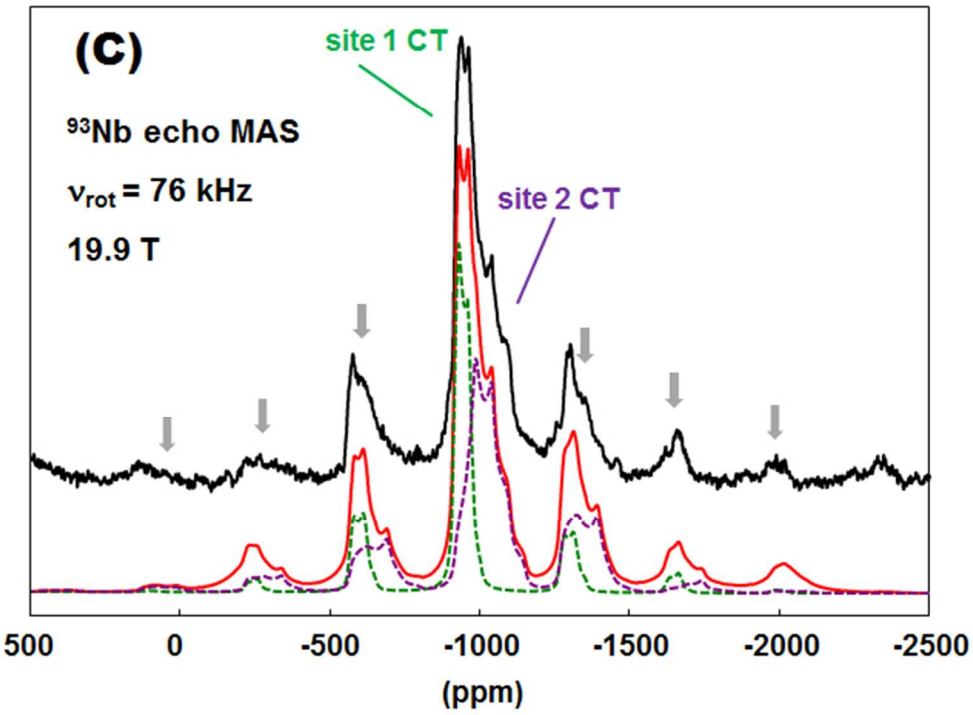


Figure 4 (C)
172x124mm (96 x 96 DPI)

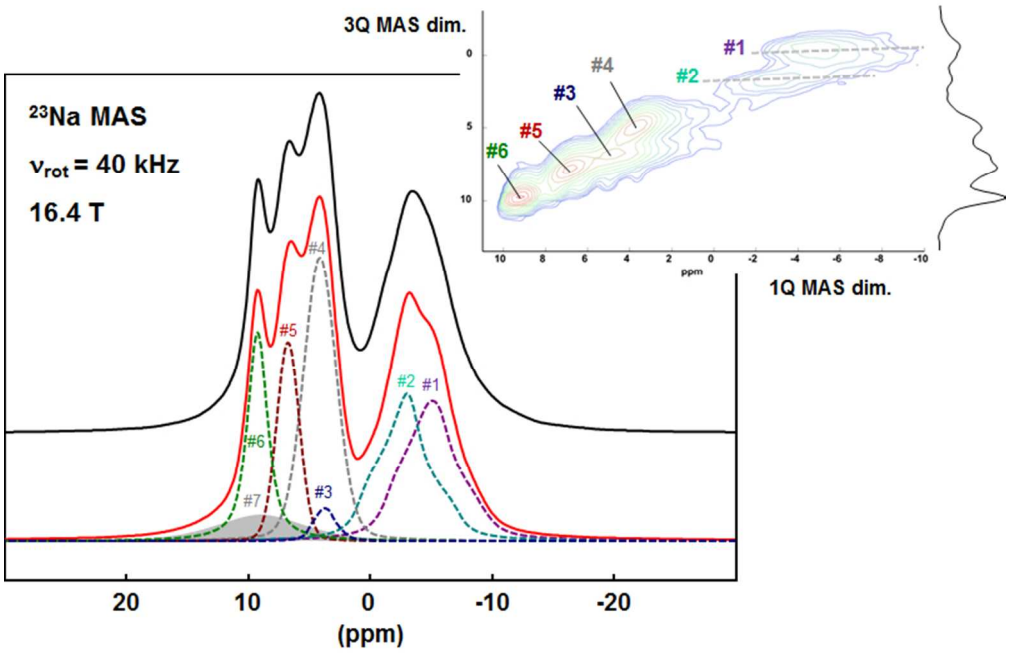


Figure 5
211x145mm (96 x 96 DPI)

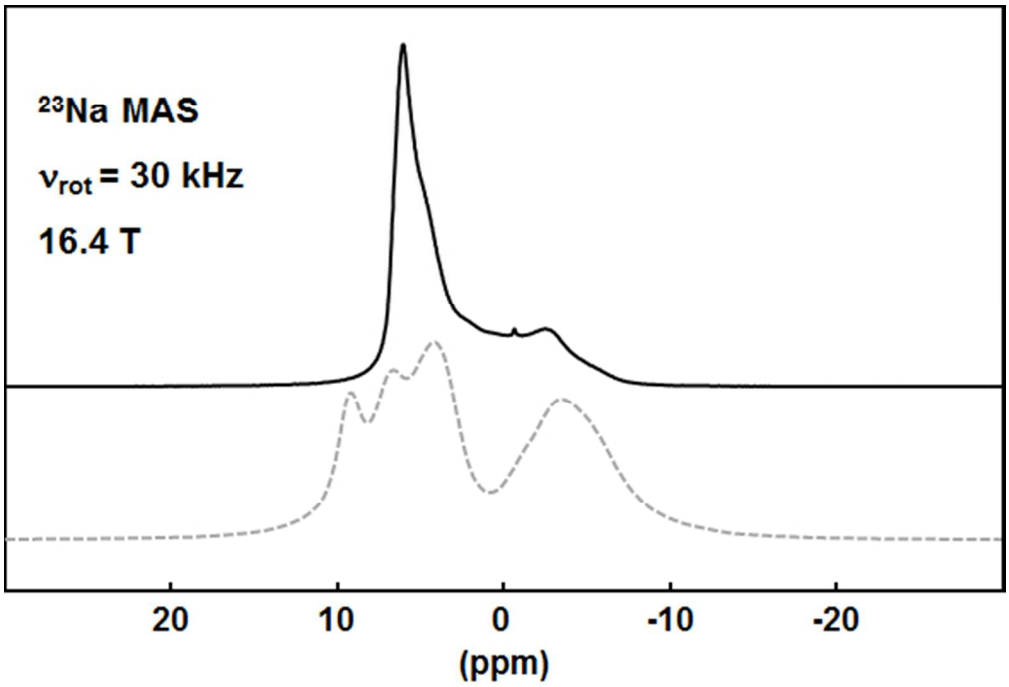


Figure 6
155x108mm (96 x 96 DPI)

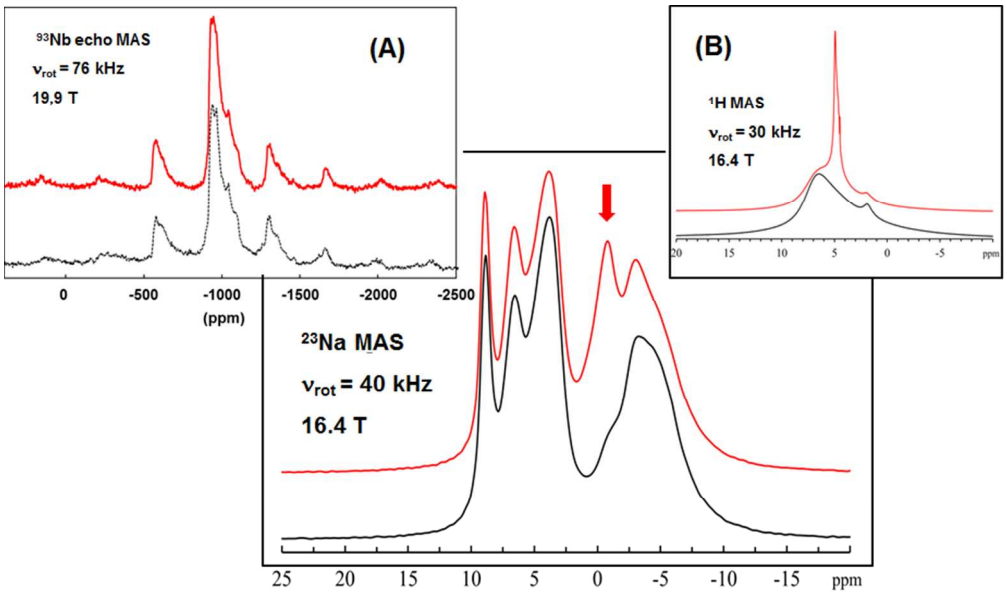


Figure 7
243x143mm (96 x 96 DPI)

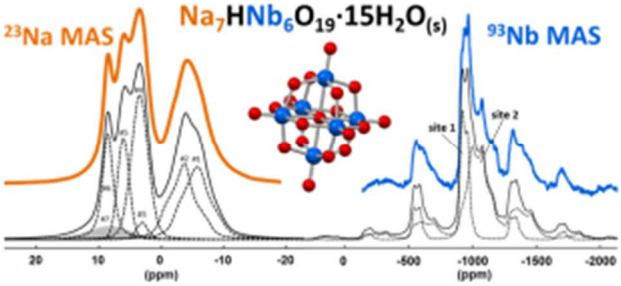


TOC graphic
81x37mm (96 x 96 DPI)